PHARMACOKINETICS AND TISSUE DISTRIBUTION OF 5,7-DIMETHOXYFLAVONE IN MICE

By

DI BEI

A DISSERTATION PRESENTED TO THE GRADUATE SCHOOL
OF THE UNIVERSITY OF FLORIDA IN PARTIAL FULFILLMENT
OF THE REQUIREMENTS FOR THE DEGREE OF
DOCTOR OF PHILOSOPHY

UNIVERSITY OF FLORIDA

2015

To the people who love me and the people that I love

ACKNOWLEDGMENTS

First and foremost, I would give special thanks to the most amazing advisor Dr. Hartmut Derendorf for wisely mentoring me, unconditionally supporting me and continuously guiding me through difficult times with incredible patience. He is so knowledgeable, fair-minded and considerate that I can never stop learning from him. I would also like to thank my supervisory committee, Dr. Guenther Hochhaus, Dr. Sihong Song and Dr. Robert W Huigens for their time and effort on advising me and helping me. I want to thank Dr. Guohua An, my previous advisor back in Orlando campus, for kindly giving me opportunity to work on PBPK project and publishing those works. Without her, the animal experiments would not be accomplished in such an efficient way.

PhD study to me is like a marathon. There have been a lot of frustrations which almost made me quit half way. Thanks to my faith as a Christian and my loving families, I could stick to my dream and able to finally reach the finish-line. So I want to take this opportunity to genuinely appreciate the love and support from them.

Finally, I want to extend my thanks to all the graduate students, post-docs, and staff in our program for being so nice and helpful. I want to share with you a poem entitled *The Road Not Taken* by Robert Frost, “Two roads diverged in a yellow wood, And sorry I could not travel both, And be one traveler, long I stood, And looked down one as far as I could, To where it bent in the undergrowth; I shall be telling this with a sigh, Somewhere ages and ages hence: Two roads diverged in a wood, and I—I took the one less traveled by, And that has made all the difference.”

TABLE OF CONTENTS

page

LIST OF TABLES

LIST OF FIGURES

LIST OF ABBREVIATIONS

2LL	Log-likelihood.
5,7-DMF	5,7-Dimethoxyflavone.
λz	Elimination rate constant in terminal phase.
ACN	Acetonitrile.
ADME	Absorption, distribution, metabolism, and excretion.
AIC	Akaike Information Criterion.
AUC	Area under the curve.
Bap	Benzo[a]pyrene.
BCRP	Breast cancer resistance protein.
BIC	Bayesian Information Criterion.
CID	Collision induced dissociation.
CL	Clearance.
CL2	Intercompartmental clearance.
Cmax	Maximal concentration.
CV	Coefficient of variance.
CWRES	Conditional weighted residual.
CYP	Cytochrome P450.
DDI	Drug-drug interaction
DV	Dependent variable.
ESI	Electro-spray ionization.
F	Bioavailability.
GC	Gas chromatography.
HPLC	High performance liquid chromatography.
IACUC	Institutional Animal Care and Use Committee.

IC50	Concentration to achieve 50% of maximal inhibition.
IPRED	Individual prediction.
I.S	Internal standard.
IV	Intravenous.
K0	Zero-order absorption rate constant.
Ka	First-order absorption rate constant.
Kp	Tissue partition coefficient.
LC-MS/MS	Liquid chromatography coupled with tandem mass spectrometry.
LLOQ	Lower limit of quantification.
MDR	Multi-drug resistance.
MRP	Multidrug resistance associated-proteins.
NCA	Noncompartmental analysis.
PBPK	Physiology-based pharmacokinetic.
PBS	Phosphate buffer saline.
PD	Pharmacodynamic.
PEG	Poly(ethylene glycol).
P-gp	P-glycoprotein.
PK	Pharmacokinetic.
PopPK	Population pharmacokinetics.
PRED	Prediction.
QC	Quality control.
QQ	Data quantile-theoretical quantile.
SE	Standard error.
TAD	Time after dose.
Tlag	Lag time in absorption.

TRAIL	Tumor necrosis factor-related apoptosis-inducing ligand.
UDPGT	Uridine diplosphate glucuronyl-transferase.
VPC	Visual predictive check.
XIC	Extracted ion chromatogram.

Abstract of Dissertation Presented to the Graduate School
of the University of Florida in Partial Fulfillment of the
Requirements for the Degree of Doctor of Philosophy

PHARMACOKINETICS AND TISSUE DISTRIBUTION OF 5,7-DIMETHOXYFLAVONE IN MICE

By

Di Bei

December 2015

Chair: Hartmut Derendorf
Major: Pharmaceutical Sciences

The purpose of this study was to investigate the PK profile of 5,7-DMF in vivo.

5,7-DMF is a natural flavonoid with many beneficial pharmacological effects. However, to date it was evaluated mainly in vitro and its PK in vivo remains largely unknown. In addition, current available quantification methods of 5,7-DMF all lack sufficient sensitivity. Therefore in our study, we established a sensitive quantification method of 5,7-DMF using LC–MS/MS. It was fully validated and accuracy, precision, sensitivity, selectivity, recovery and stability were evaluated thoroughly in mouse plasma. This quantification method was also validated in mouse tissues.

In the dose escalation study in mice, AUC was demonstrated dose proportional within the dose range 10 to 50 mg/kg 5,7-DMF. And in the following study of 10 mg/kg oral dosing, the calculated bioavailability was 13.8%. The maximal 5,7-DMF concentrations in plasma and tissues were reached within 30 min. Plasma C_{max} was 1870 ± 1190 ng/mL, and AUC_t was 532 ± 165 hr*ng/mL and terminal half-life was 3.40 ± 2.80 hr. The volume of distribution was 90.1 ± 62.0 L/kg. Clearance was 20.2 ± 7.49 L/hr/kg. Except for muscle and adipose, other tissues had higher C_{max} than plasma,

ranging from 1.75- to 9.96-fold. After oral administration, K_p of these tissues were 0.65 to 12.9.

Two-compartmental model without Tlag model best described the oral plasma data. The fitted PK parameter K_a was 6.04 1/h, V_1 was 0.05 L, V_2 was 0.56 L, CL was 0.55 L/h, and CL_2 was 0.04 L/h. This model was extrapolated to human of average body weight of 70 kg with V_1, V_2, CL and CL_2 scaled up, which may provide insight for 5,7-DMF concentration prediction in human plasma.

In conclusion, we reported for the first time the PK, tissue distribution and modeling and simulation of 5,7-DMF in mice. These results will be critical in evaluating if those beneficial in vitro effects can be translated in vivo. Ultimately, the plasma and tissue levels of 5,7-DMF can be used for PBPK modeling and can extrapolated in predicting 5,7-DMF concentrations in human.

CHAPTER 1
INTRODUCTION

Phytochemicals are more and more popular because of the potential as alternative or adjunct medicine [1-2]. Herb-drug interaction of clinically importance has gained more interest during the past years [2-5]. Especially for flavonoids abundant in fruit, vegetables and wine, they are polyphenols that can impact on cancer proliferation, inflammation, angiogenesis and metastasis [6-10]. Its pharmacological evidence of chemoprevention has been reported concerning cancer in GI tract [11-14], and liver [15], prostate [16-17], ovarian [18], lung [19], endometrial [20] and breast cancers [21-26].

5,7-Dimethoxyflavone (5,7-DMF) is a naturally-occuring flavonoid that is abundant in tropical plant sources such as Kaempferial paviflora (also known as Thai Genseng), Piper caninum and Leptospermum scoparium [27-29], all of which have been used as folk medicine to treat gastrointestinal disorder, infections and hypertension [27-28].

5,7-DMF has been evaluated extensively in vitro and the results showed that 5,7-DMF has many beneficial pharmacological activities. For example, it has anti-inflammatory activity [30], vasorelaxation and cardioprotection effect by increasing potassium efflux and inhibiting calcium influx [31], and selectively inhibitory effect against butyrylcholinesterase versus acetylcholinesterase [32]. Moreover, Walle's group conducted a series of in vitro studies to evaluate the chemotherapeutic and chemopreventive potential of this compound [33-35]. They found that 5,7-DMF can prevent hepatic carcinogenesis by inhibiting Cytochrome P450 (CYP) 1A1 activity,

which subsequently decreased the carcinogenbenzo[a]pyrene (BaP)-induced DNA adduct formation [35].

The chemopreventive effect of 5,7-DMF was also observed in human esophageal cancer cells and human oral carcinoma cells by regulating CYP1B1 activity [34-35]. 5,7-DMF was also reported to have chemosensitizing effect in hetapocellular carcinoma cells and human leukemic cells through tumor necrosis factor-related apoptosis-inducing ligand (TRAIL)-mediated apoptosis [36-37]. In addition, 5,7-DMF was shown to improve the accumulation of rhodamine 123 into the cells with overexpression of P-glycoprotein (P-gp), an efflux transporter which is present in various cancer cells and plays an important role in multi-drug resistance (MDR) [27]. In addition to P-gp inhibition, 5,7-DMF also has inhibitory effect on other two efflux transporter members - multidrug resistance associated-proteins (MRPs) and Breast Cancer Resistance Protein (BCRP). For example, 5,7-DMF can increase the accumulation of doxorubicin in A549 cells as a result of suppression of MRPs [38]. 5,7-DMF demonstrated very potent BCRP inhibition both in vitro and in vivo even at low micro molar concentrations with the in vitro IC_{50} for BCRP inhibition is 1.41 μM [39-40]. The plasma and tissue concentrations of mitoxantrone, an anticancer drug with high affinity to BCRP, were significantly increased in vivo with the co-administration of 5,7-DMF [39].

As is known, MDR is the major cause for the failure of cancer chemotherapy treatment. An important mechanism for MDR is the decreased intracellular concentration of anticancer drugs due to the overexpression of efflux transporters, including P-gp, BCRP, and MRPs [41]. The broad inhibitory effect of 5,7-DMF on P-gp,

BCRP, and MRPs makes it a very promising chemosensiting agent. Although 5,7-DMF has numerous beneficial pharmacological activities as mentioned above, it should be noted that most of the results were obtained in vitro. To evaluate if those in vitro effects can be translated in vivo, it is important to know the PK information of 5,7-DMF, especially the in vivo concentrations of 5,7-DMFat the target site(s) (i.e. tissues).

The ADME property of 5,7-DMF is promising in five major aspects. First of all, it has low toxicity against normal healthy cells with IC_{50} around 100 μM in lung BEAS-2B cells and the esophageal HET-1A cells [42] while its analog chrysin exhibited an IC_{50} of 2 μM. secondly, 5,7-DMF is a potent BCRP inhibitor as demonstrated in the literature that in vitro IC_{50} for BCRP inhibition is 1.41 μM and under 25 mg/kg doing, 5,7-DMF significantly increased the mitoxantrone levels in liver and kidney [39-40]; thirdly, it led to high tissue accumulation after doing [43-44] which makes tissues interesting site for researching 5,7-DMF's PK and PD. Fourthly, it had improved intestinal absorption and metabolic stability [44]. Compared to other methylated and unmethylated flavonoids, 5,7-DMF demonstrated the highest stability when exposed to human liver hepatocyte, human liver microsome and human liver S9 fraction [45-47]; Besides, methylated flavones showed approximately 5- to 8-fold higher apparent permeability. The high metabolic stability in addition to increased intestinal absorption of the methylated polyphenols make them more promising and interesting than the unmethylated polyphenols as potential chemopreventive compounds. [47].

However, to date there still have been large knowledge gap about this compound. Primarily, the information related to the in vivo PK of 5,7-DMF is very limited [43-44]. In addition, to the best of our knowledge, there are only two quantification

methods of 5,7-DMF that have been published, both of which lack sufficient sensitivity, with one of them reported lower limit of quantification (LLOQ) of 1860 ng/mL using HPLC and the other method reported LLOQ of 800 ng/mL in non-biological matrices using gas chromatography (GC) [44, 48]. In order to better understand the pharmacokinetics of 5,7-DMF in vivo, especially to capture its terminal phase, a more sensitive quantification method is needed. The purpose of our study was to establish and validate a sensitive quantification method of 5,7-DMF in biological matrices such as mouse plasma and mouse tissues using LC–MS/MS assay, to apply this quantification method evaluate the PK profile of 5,7-DMF in mouse and finally to construct PK model based on it. And the objectives for 5,7-DMF project is listed as followed:

Specific Aim 1

The first aim is to develop and validate a new bioassay to sensitively and accurately quantify 5,7-DMF in mice matrices such as plasma, and other tissues. This aim will be accomplished in Chapter 2. The significance and innovations of this chapter will be, (i). Analytical methodology using liquid chromatography tandem mass (LC-MS/MS) to quantify 5,7-DMF is new. Once established, the sensitivity will be greatly improved compared to previously reported methods using HPLC and GC; (ii). The matrix effect and recovery yield will be first reported; and (iii). The assessment of 5,7-DMF stability in biological matrix is novel. Our assay will provide basis for future PK sample analysis.

Specific Aim 2

The second aim is to establish PK profiles and tissue distribution of 5,7-DMF in mice for the first time. This aim will be accomplished in Chapter 3. The significance and innovations of this chapter will be, (i). Dose linearity of 5,7-DMF has not been

investigated; (ii). Bioavailability in mice has not been reported; and (iii). Tissue distribution profile remained unknown.

Specific Aim 3

The third aim is to construct the PK model based on the mouse plasma PK profile and extrapolate this model to human species in order to predict the human plasma level of 5,7-DMF. This aim will be accomplished in Chapter 4. The significance and innovations of this chapter will be, (i). Up to date, the literature on PK model of 5,7-DMF is missing so our work will be the first to initiate PK modeling on 5,7-DMF; (ii). Our model will be the first to explain and predict 5,7-DMF in vivo; and (iii). This will be further utilized in building PBPK modeling for clinical relevance.

As learnt from previous literature, 5,7-DMF could reverse BCRP-mediated MDR in mouse tissues [13-14], but in clinical trials, it is fairly difficult to measure tissue concentrations. In this regard, PBPK is advantageous over traditional PK method in that it consists of physiologically-meaningful compartments so that the tissue concentrations can be accurately predicted. The ultimate goal is to extrapolate the PBPK model in mice to human in order to simulate the 5,7-DMF levels in human plasma and most importantly, the accumulations in tissues where 5,7-DMF had the promising PD effect.

CHAPTER 2
DEVELOPMENT AND METHOD VALIDATION OF BIOANALYTICAL METHODS

Background

For the beneficial pharmacological effects of 5,7-DMF mentioned above, it should be noted that most of the data were obtained from in vitro studies. The information of the bioavailability of 5,7-DMF, as well as its pharmacokinetics (PK), is critical for estimating whether the concentrations tested in vitro are physiologically relevant and whether those in vitro effects can be translated in vivo. However, before our study there are only two quantification methods of 5,7-DMF that have been published, both of which lack sufficient sensitivity, with one of them reported a lower limit of quantification (LLOQ) of 1860 ng/mL using HPLC and the other method reported a LLOQ of 800 ng/mL using gas chromatography (GC) [44, 48]. As is generally agreed, sensitive and accurate bioassay is the key to profile PK and PD [49]. In order to better understand the pharmacokinetics of 5,7-DMF in vivo, especially to capture its terminal phase, a more sensitive quantification method is needed. The purpose of our study in this chapter was to establish and validate a sensitive quantification method of 5,7-DMF using LC–MS/MS assay, and to evaluate the PK of 5,7-DMF in mouse.

LC-MS/MS is a state-of-art technique which coupled high performance liquid chromatogram with triple quadruple to separate analyte from other substances based on different retention time in HPLC and different m/z after fragmentation inside of mass spectrometer. This type of bioassay is widely used in preclinical and clinical sample analysis [50]. Since LC-MS/MS has been reported as fast, sensitive and selective method which can generate reliable and efficient data out of plasma, urine and tissues [51-53], it was chosen for this study as the main bioassay.

The innovations and significance therefore include but not limited to, (i). Analytical methodology using liquid chromatography tandem mass (LC-MS/MS) to quantify 5,7-DMF is novel; Once established, the sensitivity will be greatly improved compared to previously reported methods using HPLC and GC; (ii). The matrix effect and recovery yield will be first reported; (iii). The assessment of 5,7-DMF stability in biological matrix is novel. Our assay will provide basis for future PK sample analysis.

Materials and Methods

Reagents and Chemicals

5,7-DMF (>99%) and 5,7,4-trimethoxyflavone (TMF, >99%) were purchased from Indofine Chemical Company, Inc. (Hillsborough, New Jersey, US). Ammonium formate (99%) was obtained from ACROS Organics (New Jersey, US). Analytical HPLC grade acetonitrile (ACN), water and formic acid were purchased Fisher Scientific (Pittsburg, Pennsylvania, US). Analytical spectrophotometric grade ethyl acetate (99.5%) was obtained from Alfa Aesar (Ward Hill, Massachusetts, US). Heparin-treated mouse plasma was purchased from BioreclamationIVT (East Meadow, New York, US). (2-Hydroxypropyl)-β-cyclodextrin and poly(ethylene glycol) Mn 400 (PEG400) were purchased through Sigma–Aldrich (St. Louis, Missouri, US). Heparin injectable (1000 U/mL) was purchased from Patterson Vet Generics (Devens, Massachusetts, US).

Instrument Conditions

HPLC conditions

High performance liquid chromatogram (HPLC) was performed with Agilent 1200 series systems (Agilent, California, US) that include a 1260 degasser, a 1260 binary pump, a 1260 autosampler and a 1290 thermostat. 5,7-DMF and TMF were separated by Agilent XDB C18 column (4.6 mm × 50 mm, 1.8 μm particle size, Agilent, California,

US) coupled with Agilent XDB C18 guard column (2.1 mm × 5 mm, 1.8 μm particle size, Agilent, California, US) under an isocratic elution at a flow rate of 0.4 mL/min. The mobile phase is 50/50 (v/v) of 20 mM ammonium formate in water (containing 0.1% formic acid)/acetonitrile (containing 0.1% formic acid). It takes 5 μL of the aliquot and 5 min for each injection.

MS/MS conditions

5,7-DMF and I.S was monitored under positive mode by Agilent 6460 triple quadruple (Agilent, California, US) equipped with Agilent Jet Stream electrospray ionization (AJS ESI). In multiple reaction monitor (MRM) mode, transition ion pair for 5,7-DMF is m/z 283 > m/z 239 while the transition ion pair for I.S is m/z 313 > m/z 298. To obtain the optimal sensitivity, the fragmentor is 120 V for both 5,7-DMF and I.S, and the collision energy are 33 V and 25 V for 5,7-DMF and I.S, respectively. The mass spectrometer was operated at the gas temperature of 300 °C, gas flow of 8 L/min, nebulizer of 35 psi, sheath gas temperature of 400 °C, sheath gas flow of 11 L/min, capillary voltage of 4500 V and cell accelerator voltage of 7 V. The response acquisition was performed using MassHunter Data Acquisition software and the qualitative analysis was done with MassHunter Qualitative Analysis software (Version B 6.0). Then the quantitative analysis was performed by MassHunter QQQ Qualitative Analysis software (Version B 6.0).

Sample Preparation of Calibration Standards and Quality Control for LC–MS/MS

TMF was chosen as the internal standard (I.S) because it has similar chemical structure as that of 5,7-DMF. Stock solutions of 5,7-DMF and I.S at concentration of 1 mg/mL were prepared separately in ACN and stored in a −80 °C freezer. Intermediate working solutions of 5,7-DMF were prepared by serial dilution with mobile phase (neat

solution). Prepared 10-fold intermediate working solutions of analyte by serial dilution with mobile phase from 10 µg/mL working solution (range: 10, 20, 50, 100, 200, 500, 1000, 2000, 5000 and 10000 ng/mL). Calibration curve in mobile phase was prepared by 10 µL of each intermediate working solutions and 10 µL IS together with 80µL mobile phase. After calibration curve in mobile phase (not shown) indicated linearity, calibration curve in mouse plasma was prepared by spiking 10 µL of intermediate working solutions and 10 µL I.S into 100 µL of blank mouse plasma. After vortex mixing for 1 min, 600 µL of ethyl acetate was added for liquid-liquid extraction on a mechanical shaker for 5 min. the liquid-liquid extraction agent was ethyl acetate which can form two immiscible layers with water phase. Then the supernatant layer was transferred to clean tubes after the centrifuge at 17,000 rpm under 4 °C for 4 min, and placed under nitrogen for evaporation. The residue was reconstituted with 100 µL of mobile phase and centrifuged at 17,000 rpm under 4 °C for 4 min to get rid of precipitation. After reconstitution, 5 µL of the sample was injected to the LC–MS/MS. Standards were prepared at concentrations 2–1000 ng/mL. Quality control (QC) samples were prepared the same way as the standards and at the concentrations of 2, 5, 50 and 500 ng/mL. Data were quantified with MassHunter QQQ Quantitative Analysis (Version B 6.0).

Assay Validations in Mouse Plasma

The intra-run/within-run validation was performed on concentrations of 2, 5, 50 and 500 ng/mL with six replicates for each concentration. And the inter-run/between-run validations were evaluated at 3 separate days with triplicates during each day on each of the concentration at 2, 5, 50 and 500 ng/mL. For separate validations, separate standard curves were freshly prepared. The standard curves were fitted by a linear regression and the validation samples were calculated back by the calibration curve of

that day. The mean and the coefficient of variance (CV) were calculated accordingly. Accuracy was calculated by comparing calculated concentrations to corresponding nominal ones.

Matrix Effect and Recovery Yield in Mouse Plasma

Standards in mobile phase/neat solution, pre-extracted spiked samples and post-extracted spiked samples were prepared in triplicate at concentrations of 2, 5, 50 and 500 ng/mL to analyze the matrix effect and recovery yield of the 5,7-DMF in mouse plasma following liquid–liquid extraction with ethyl acetate. The blank mouse plasma used was the heparin-treated mouse plasma was purchased from BioreclamationIVT (East Meadow, New York, US). Group A: 5,7-DMF and I.S were prepared directly with mobile phase without any matrix or extraction. Group B: 5,7-DMF and I.S were spiked into blank mouse plasma followed by liquid–liquid extraction, centrifugation, and reconstitution process (as described in Section 2.3). Group C: 5,7-DMF and I.S were spiked in the extracted matrix of blank mouse plasma to prepare the final concentrations of 2, 5, 50 and 500 ng/mL. Matrix effect (%) = C × 100/A and recovery (%) = B × 100/C, where A = absolute response obtained from standards mobile phase; B = absolute response obtained from pre-extracted spiked samples; C = absolute response obtained from post-extracted spiked samples.

Stability of 5,7-DMF in Mouse Plasma

Stability of 5,7-DMF in stock solution

Freshly prepared 5,7-DMF solution (1 mg/mL) and the stored DMF solution (1 mg/mL) were diluted to 500 ng/mL with mobile phase with six replicates in each group. The final concentration of the I.S is 1000 ng/mL. 5,7-DMF concentrations were compared by calculating the ratio of 5,7-DMF to I.S response.

Freeze–thaw stability of 5,7-DMF in mouse plasma

5,7-DMF solution was spiked into mouse plasma to prepare final concentrations of 2, 5, 50, 500 ng/mL and then stored in the −80 °C freezer. These samples went through one, two or three sequential freeze–thaw cycles respectively prior to sample analyses using LC–MS/MS (as described in Section 2.3). During each cycle, the samples were thawed under room temperature (25 °C) for 60 min before re-frozen and stored at −80 °C, and the next cycle happened after 24 h interval. Samples were prepared in triplicates for each concentration of each cycle set.

Long-term stability of 5,7-DMF in mouse plasma

5,7-DMF solution was spiked into mouse plasma to prepare final concentrations of 2, 5, 50, 500 ng/mL and then stored in −80 °C freezer for up to 14 days. At Days 4, 7 and 14, samples in triplicates were analyzed and compared with freshly prepared plasma samples.

Short-term temperature stability of 5,7-DMF in mouse plasma

The short-term stability was conducted by measuring triplicate freshly prepared QC samples at concentrations 2, 5, 50 and 500 ng/mL in mouse plasma versus those QC samples at the same concentrations placed on bench top for 24 h.

Post-preparative stability of 5,7-DMF

On Day 1, standards in mouse plasma and QC samples in triplicates were prepared and placed in autosampler for quantification. The autosampler remained the temperature control of 4 °C all the time. After 24 h sitting inside the autosampler, the same QC samples were re-analyzed on Day 2 by the instrument and the concentration was re-determined by the standard of Day 1. The calculated concentrations in Day 2 were compared in parallel with those in Day 1.

Validation of Quantification Method in Tissues

For tissue samples, tissue was weighed and added PBS buffer (pH=7.4) based on 10-fold volume of each tissue weight. They were cut into smaller pieces before homogenization. Then 10 µL of I.S was spiked into 100 µL of tissue homogenate. Other steps were the same as plasma sample preparation. When validating the LC-MS/MS methods in tissues, QC sample preparation followed the same procedure of calibration curve. And the QC concentrations were selected at 2 and 500 ng/mL, which represented the lower and higher end of the tissue PK samples.

Results

Determination of 5,7-DMF and I.S by LC–MS/MS

To acquire the mass spectra of analyte and I.S, 1000 ng/mL of 5,7-DMF and I.S were prepared separately with mobile phase. Then 5 µL of each was injected into LC–MS/MS and infused with 0.4 mL/min flow rate of the mobile phase. The analyte and I.S were monitored under MRM in positive mode for good ionization. The chemical structures of analyte and I.S were shown in Fig. 2-1. The full scan and the proposed ion fragmentations of 5,7-DMF and I.S was shown in Fig. 2-2. The analyte exhibited the precursor ion of m/z 283 (Fig. 2-2A) corresponding to the protonated form [M+H]+ of the compound with the molecular weight of 282. The precursor ion of 283 was chosen over 305 is because of higher intensity. This form of ion is quite typical in positive mode on the compounds prone to get a proton and become protonated. After collision induced dissociation (CID), the resulting product ion has a unimodal peak and a predominant m/z of 239 (Fig. 2-2B). The 44 Da loss compared with the precursor ion was possibly due to the loss of CO2 group from the molecule. But it was also possible some other groups were lost during the dissociation process. The CO2 group proposed here is only

putative hypothesis waiting to be confirmed with future experiment. The I.S exhibited the precursor ion of m/z 313 (Fig. 2-2C) corresponding to the protonated form of the compound with the molecular weight of 312. Again, I.S precursor ion of 313 was chosen over 335 because of more abundance which led to possibly higher intensity of product ion. After CID, the resulting product ion of the I.S has a fragment ion with m/z of 298 (Fig. 2-2D), with a loss of 15 Da likely because of dissociation of radical group CH3 radical dot. Based on the full scan of Thus for the transition channel, the ion pairs chosen for the analyte and I.S are m/z 283 → 239 and m/z 313 → 298, respectively.

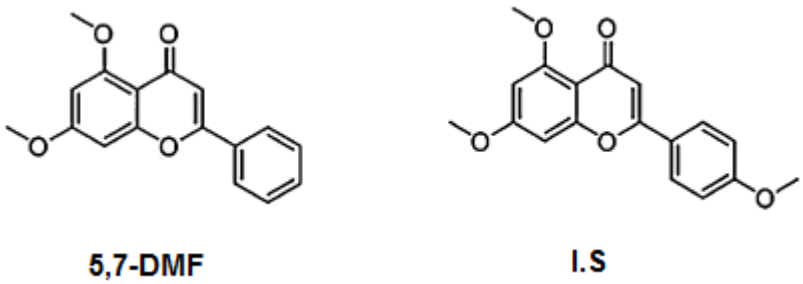

Figure 2-1. Chemical structure of 5,7-DMF and I.S

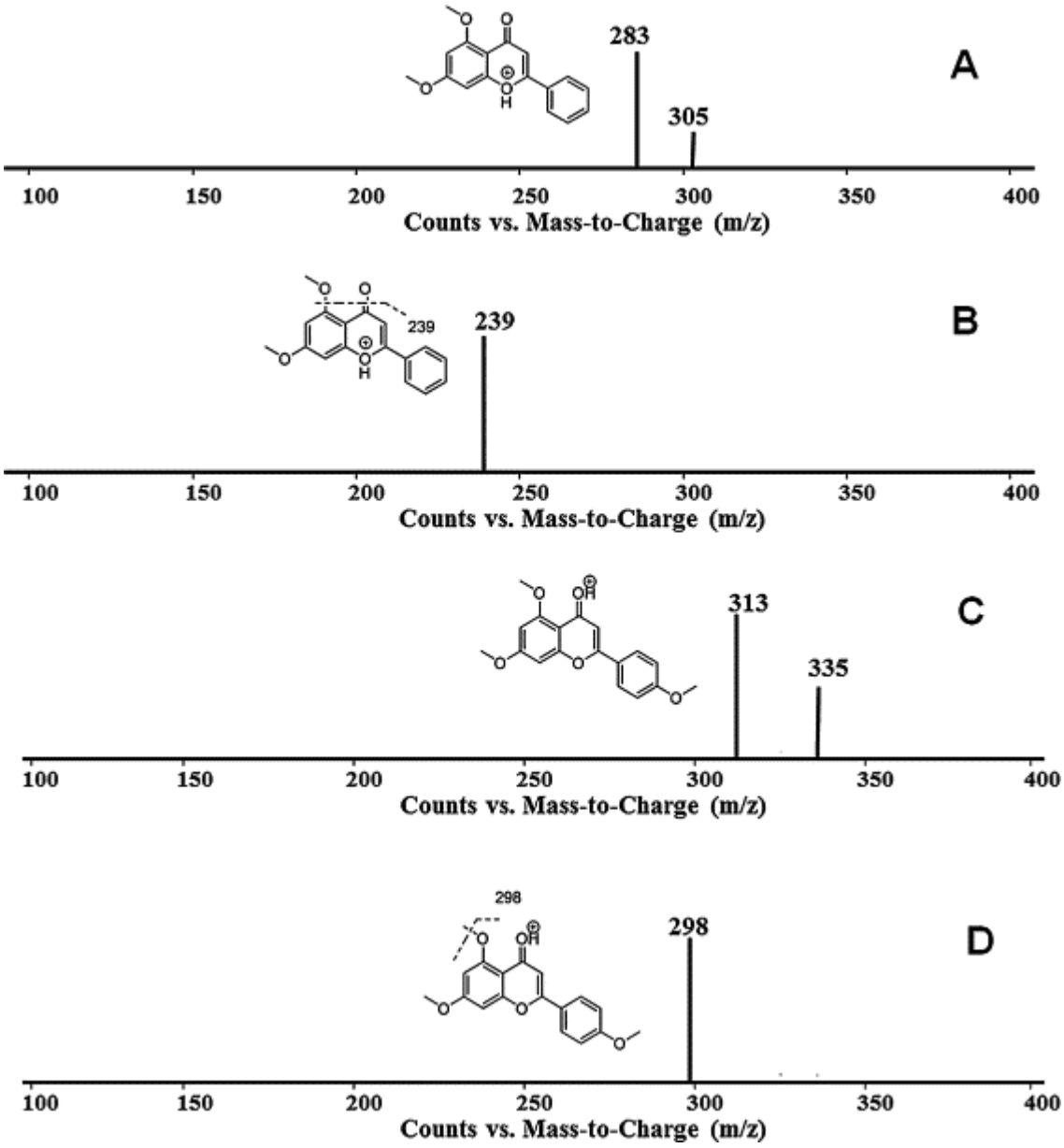

Figure 2-2. Mass spectra of 5,7-DMF and I.S.

Liquid–liquid extraction method was chosen because of following three benefits it offers. First of all, it excludes the water-soluble sodium and potassium which can be detrimental to the instrument due to involatile property. Secondly, it results in higher extraction and lower LLOQ than the protein precipitation method for 5,7-DMF. Thirdly, samples can be condensed through liquid–liquid extraction, which is very beneficial to those samples with concentration range between LOD and LLOQ and cannot be detected otherwise. The mobile phase of 50/50 (v/v) of 20 mM ammonium formate in water (containing 0.1% formic acid)/acetonitrile (containing 0.1% formic acid) was chosen based on good peak shape and retention time of the analyte and I.S. The mass spectrometer was operated at the gas temperature of 300 °C, gas flow of 8 L/min, nebulizer of 35 psi, sheath gas temperature of 400 °C, sheath gas flow of 11 L/min, capillary voltage of 4500 V and cell accelerator voltage of 7 V. These parameters were optimized by the built-in software MassHunter Optimizer. The parameters that led to highest ion pair abundance and signal response were recorded and chosen. The Agilent XDB C18 column (4.6 mm × 50 mm, 1.8 μm particle size), a reverse-phase column, was used to separate the analyte from the endogenous interferences in mouse plasma. As shown in Fig. 3, reconstituted residues of 5,7-DMF in mouse plasma demonstrated the specificity of this method to detect and measure 5,7-DMF. The extracted ion chromatogram (XIC) of 5,7-DMF (Fig. 2-3A) has a single peak with the retention time of 3.7 min in blank mouse plasma through channel m/z 283 → 239. XIC of I.S (Fig. 2-3B) has a single peak with the retention time of 3.6 min in blank mouse plasma through channel m/z 313 → 298. The retention time is consistent with the hydrophobicity of the compounds. Although the analyte and I.S in this case have similar retention time, their

mass chromatograms clearly distinguish from each other as they have very different transition ions. Thus there were no shoulder peaks or split peaks observed in any XIC of the analyte or I.S, which means there was no interference from other compounds or matrix during the quantification of either 5,7-DMF or the I.S. In addition, there was no carryover effect observed within the concentration range of the calibration curve in mouse plasma.

The LC-MS/MS method established in mouse plasma has good linearity of greater than 0.99, as shown in Fig. 2-4, with weighted factor of $1/x^2$.

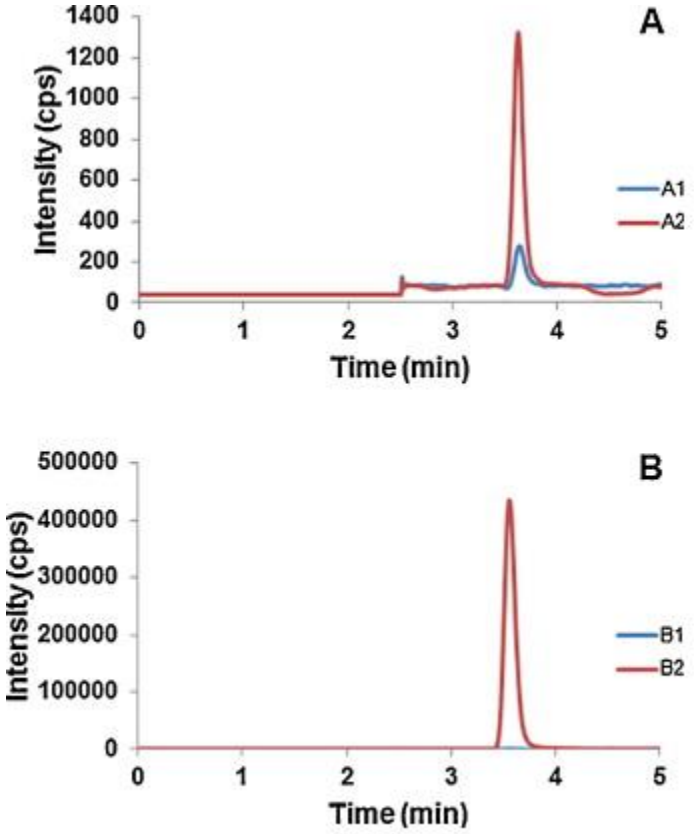

Figure 2-3. XIC of the 5,7-DMF (2 ng/mL) and I.S (1000 ng/mL) in mouse plasma. A1 was XIC signal of analyte in blank mouse plasma; A2 was XIC signal of analyte at 2 ng/mL in mouse plasma. B1 was XIC signal of I.S in blank mouse plasma; B2 was XIC signal of analyte at 1000 ng/mL in mouse plasma.

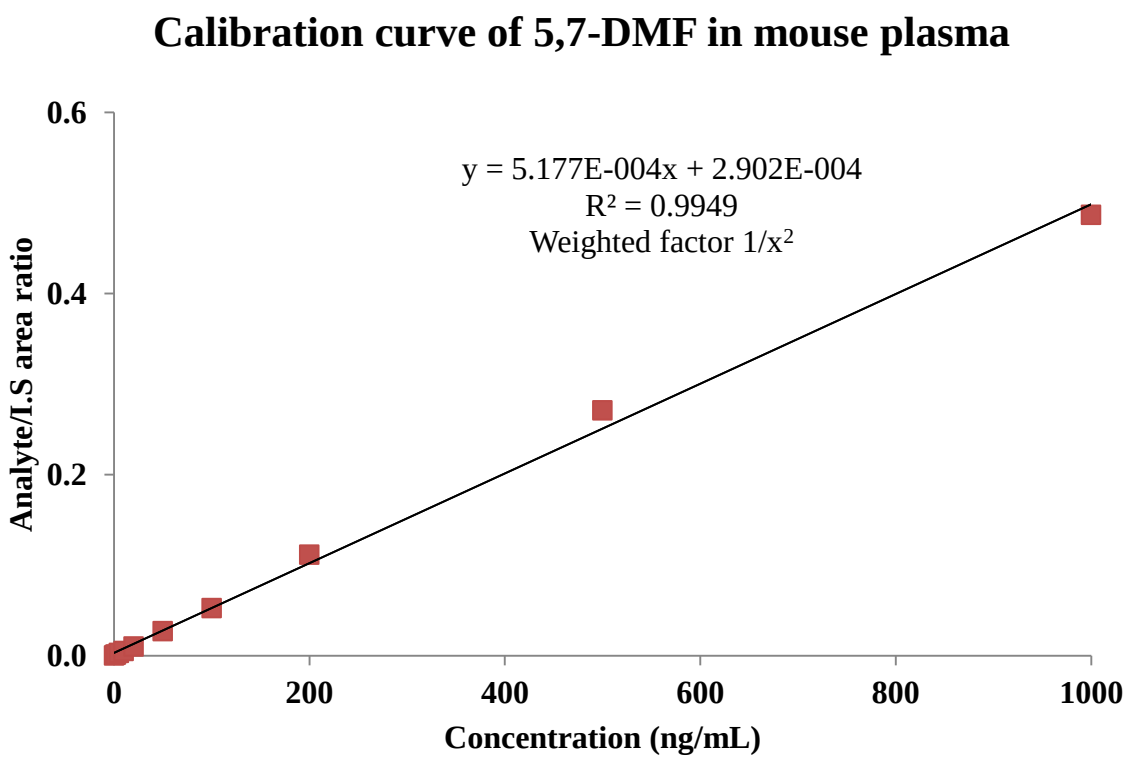

Figure 2-4. Calibration curve of 5,7-DMF in mouse plasma.

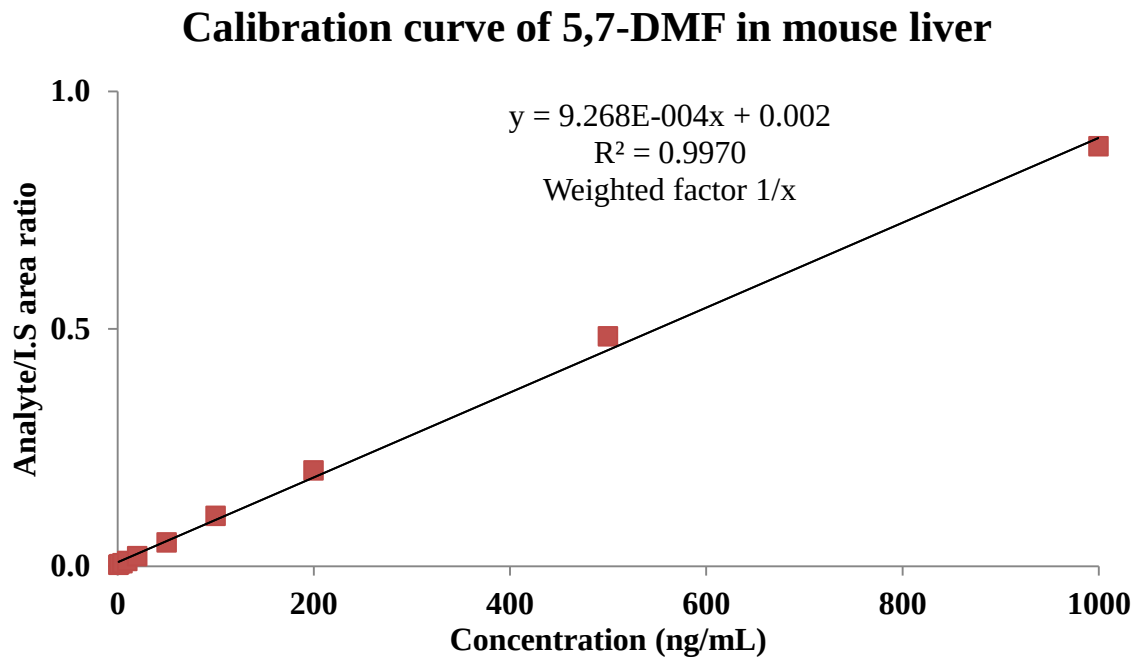

Figure 2-5. Calibration curve of 5,7-DMF in mouse liver.

Method Validation

Based on the method described above, the calibration curve has a linearity of 2–1000 ng/mL. The limit of detection for this method is 1 ng/mL with signal-to-noise (S/N) ratio of greater than 3, and the lower limit of quantification for this method is 2 ng/mL with S/N ratio greater than 5. It was fully validated for concentrations of 2, 5, 50 and 500 ng/mL by six replicates for each concentration during intra-run validation and triplicate for each concentration during three inter-run validations. The accuracy and precision were presented in Table 2-1 and Table 2-2. The accuracy for intra-run validation was from 94.4% to 106% with CV% ranging from 0.50% to 4.60%. The accuracy for inter-run validation was from 100% to 107% with CV% ranging from 2.71% to 9.07%. As shown in Table 2-1 and Table 2-2, the means and CVs for all concentrations were within ±15% difference, including LLOQ. According to FDA guideline [54], the accuracy and precision should be within ±15% of the nominal concentrations except for the LLOQ, which should be within ±20%.

Table 2-1.Intra-day (within-day) validation of 5,7-DMF in mouse plasma (N=6).

Concentration in mouse plasma (ng/mL)	Mean conc. (ng/mL)	Accuracy (%)	CV (%)
2	1.89	94.4	4.60
5	4.93	98.5	2.65
50	52.8	106	3.47
500	490	97.9	0.50

Table 2-2. Inter-day (between-day) validation of 5,7-DMF in mouse plasma (N=3*3).

Concentration in mouse plasma (ng/mL)	Mean conc. (ng/mL)	Accuracy (%)	CV (%)
2	2.01	100	9.07
5	5.21	104	3.03
50	53.3	107	2.99
500	510	102	2.71

Matrix Effect and Recovery Yield

Standards in mobile phase/neat solution, pre-extracted spiked samples and post-extracted spiked samples were prepared in triplicate analyze the matrix effect and recovery yield. Based on the data shown in Table 2-3, the matrix effect and recovery yield of 5,7-DMF in mouse plasma were 86.8–99.8% and 87.4–99.8%, respectively. Currently, there are no guidelines for the criteria of matrix effect and recovery yield. The matrix effect within ±15% is generally accepted. In this case, the quantification method had a consistent matrix effect throughout low, medium and high concentrations of the calibration curve, which indicated that this method has little or negligible ion suppression. The recovery yield was proved consistent (87.4–99.8%) through different concentrations, indicating the high extraction efficiency if this method.

Table 2-3. Matrix effect and recovery yield of 5,7-DMF in mouse plasma (N=3).

Concentration (ng/mL)	Matrix effect (mean±SD)	Recovery yield (mean±SD)
2	99.8±10.1	99.8±2.41
5	92.8±0.66	100±2.97
50	88.9±1.38	90.4±1.70
500	86.8±0.86	87.4±0.99

Stability of 5,7-DMF

Stability of 5,7-DMF in stock

To investigate the stability of 5,7-DMF stock solution stored in the −80 °C freezer, freshly prepared 5,7-DMF solution was compared with stock solution that had been stored in the freezer for 2 months. The mean ratio of stored solutions to freshly prepared 5,7-DMF was 0.86 (or 86%). The analysis result indicated that the degradation of the stock solutions in the freezer is less than 15% compared to freshly prepared 5,7-DMF solutions. Based on the result, the stored stock 5,7-DMF solutions were stable.

Freeze–thaw stability of 5,7-DMF in mouse plasma

The results in Table 2-4 showed that different concentrations of 5,7-DMF in mouse plasma going through up to three freeze–thaw cycles, the degradation of the analyte was all within 15%. Therefore, the results were reliable since the analyte was stable for three freeze–thaw cycles.

Table 2-4. Freeze-thaw stability of 5,7-DMF in mouse plasma (N=3).

Freeze-thaw cycle	5,7-DMF Concentration (ng/mL)	Ratio to freshly prepared samples
1	2	105
1	5	105
1	50	94
1	500	96
2	2	86
2	5	86
2	50	107
2	500	112
3	2	93
3	5	92
3	50	103
3	500	99

Long-term stability of 5,7-DMF in mouse plasma

5,7-DMF at concentrations of 2, 5, 50 and 500 ng/mL in mouse plasma were stored in −80 °C freezer for up to 2 weeks (14 days) before analyzed. The stability results in Table 2-5 indicated that the changes in the analyte concentration were within 15% compared with freshly prepared mouse plasma samples of same nominal concentrations. Thus the plasma samples were stable in the storage conditions for up to 14 days. Since this period exceeded the time interval between the time of first plasma sample collected and the time of last sample analyzed, the PK study results were reliable.

Table 2-5. Long term stability of 5,7-DMF in mouse plasma (N=3).

Storage duration (Day)	5,7-DMF Concentration (ng/mL)	Ratio to freshly prepared samples
4	2	105
4	5	88
4	50	93
4	500	108
7	2	97
7	5	96
7	50	90
7	500	104
14	2	103
14	5	98
14	50	88
14	500	97

Short-term temperature stability of 5,7-DMF in mouse plasma

The results shown in Table 2-6 indicated that the ratio of analyte-to-I.S in prepared samples that were exposed to room temperature for 24 h to the ratio in freshly prepared samples were between 94 and 102, indicating the degradation was less than

5%. Within 24 h on the bench top, plasma samples preparation was finished. Therefore, the samples were considered stable during preparation.

Table 2-6. Short term temperature stability of 5,7-DMF in mouse plasma (N=3).

Concentration (ng/mL)	Ratio to freshly prepared samples
2	100
5	102
50	94
500	102

Post-preparative stability of 5,7-DMF

The results in Table 2-7 demonstrated that the ratios of QC concentrations of Day 2 were between 103 and 113 compared with those calculated of Day 1. Since the whole batch of PK samples were finished running within 24 h, the measured were considered stable within 24 h during the resident time inside the autosampler after preparation.

Table 2-7. Post-preparative stability of 5,7-DMF (N=3).

Concentration (ng/mL)	Concentration on Day 1 (ng/mL)	Concentration on Day 2 (ng/mL)	Mean ratio to Day 1
2	1.88±0.14	2.13±0.07	113
5	4.99±0.17	5.24±0.17	105
50	51.5±1.81	54.0±1.93	105
500	488±2.24	502±1.00	103

Validation of quantification method in tissues

As reported, our LC-MS/MS quantification method on mouse plasma was proven to be accurate, reliable, fast, sensitive and selective [55]. It was fully validated and the precision and accuracy of various QC samples all passed the criteria based on FDA guideline [54, 56]. In this study, it was applied and validated in tissue matrices. As indicated by the FDA guideline and the newest draft guidance [54, 56], the change in

the biological matrices within same species is the typical method modification and only partial validation is needed. Further, it is indicated in these guidance that, the total number of QC samples should be either 5% of the total samples to be analyzed or at least 6 QC samples in total, whichever number is greater [54, 56]. Therefore, in this case, for each tissue analysis, we performed intra-day validations on various concentrations with each concentration in triplicates (N=3) and the method validation results were shown in Table 2-8.

The LC-MS/MS methods in mouse tissues had calibration curves with good linearity, as indicated by high R^2 values of greater than 0.99. Fig. 2-5 to Fig. 2-13 represented mouse liver, kidney, intestine, brain, spleen, heart, lung, muscle and fat. Except mouse spleen, muscle and fat, most calibration curves were captured in one linear relationship to describe concentrations between 2 and 1000 ng/mL. For spleen, muscle and fat, the calibration curves were split into 2 segments on the concentration of 100 ng/mL. Panels A represented lower calibration curves from 2 to 100 ng/mL whereas Panels B represented higher calibration curves from 100 to 1000 ng/mL.

Our results indicated QC samples at LLOQ were within 20% of the nominal concentrations and QC samples at higher concentrations were within 15% of the nominal concentrations. Thus these quantification methods were successfully validated and sample analyses using these assays were reliable. The XIC of 5,7-DMF in tissue samples were shown in Fig. 2-14.

The sample preparation method for tissue samples was optimized based on the comparison of four tissue preparation methods from a pilot study. In method A, 70% ice cold methanol was used as homogenate buffer then ethyl acetate was added prior to

the liquid-liquid extraction. In method B, PBS buffer was used as the homogenate buffer. 500 µL of acidified acetonitrile (acetonitrile with 0.2% formic acid) was added for further protein precipitation. The samples were placed in -20ºC freezer for 5 min before centrifugation. The supernatant layer was dried and reconstituted prior to injection. In method C, acidified methanol was used as the protein precipitation agent. Other steps were the same as that in method C. In method D, PBS buffer was used as the homogenate buffer and ethyl acetate was added for extraction. The detailed comparison of these four extraction methods was listed in Table 2-9.

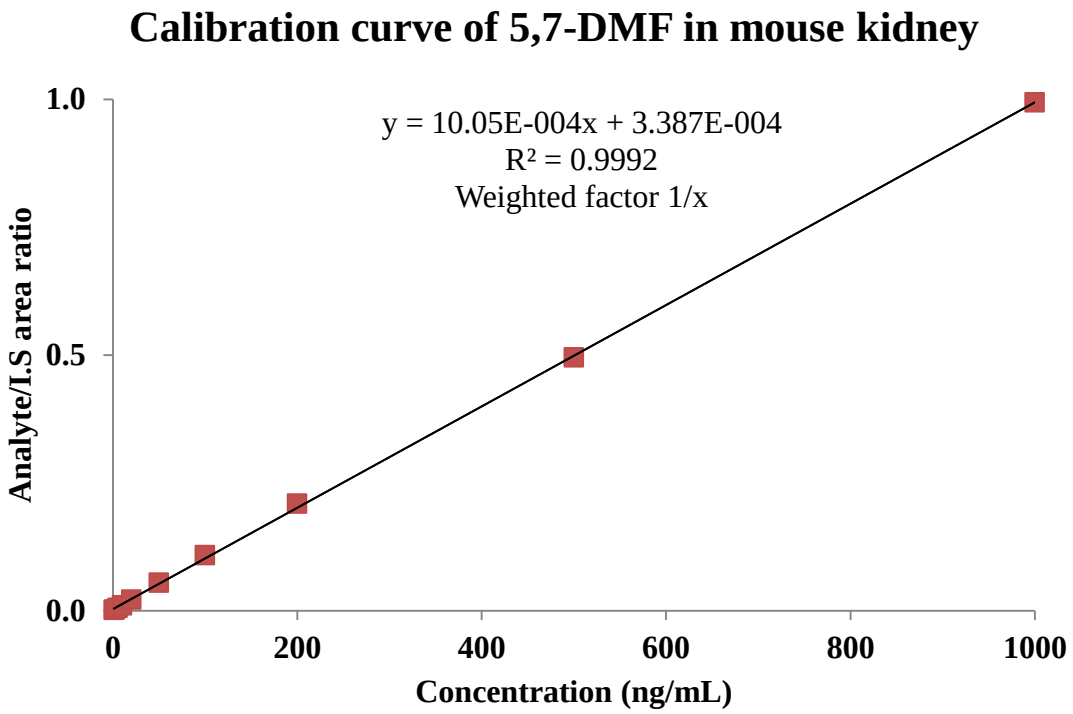

Figure 2-6. Calibration curve of 5,7-DMF in mouse kidney.

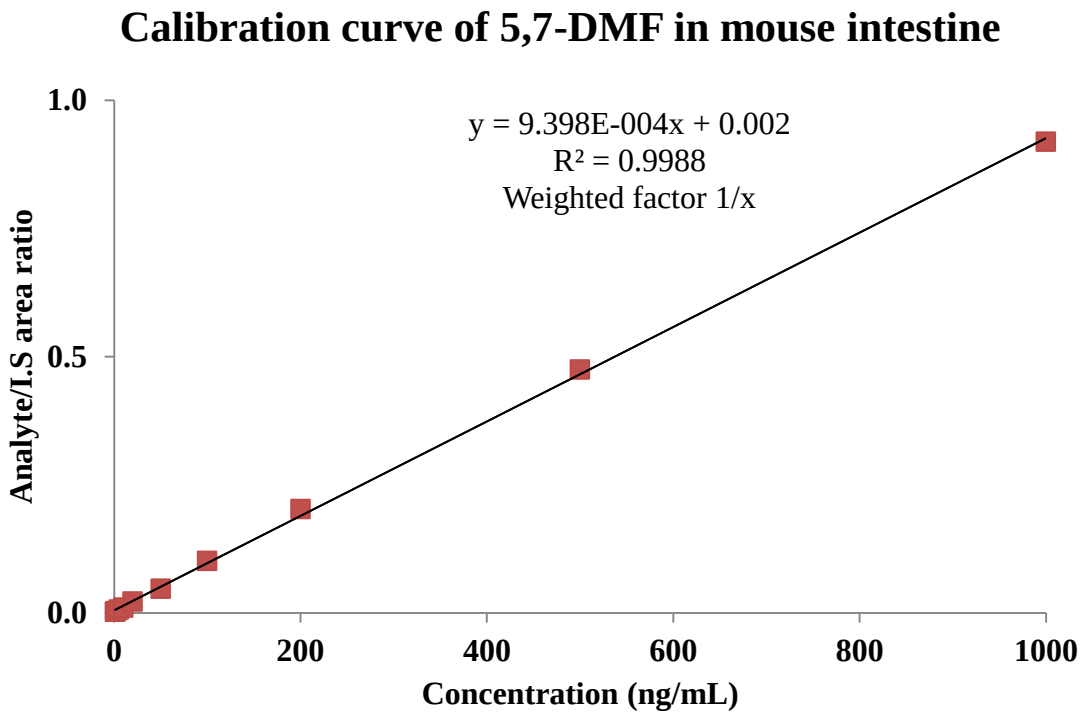

Figure 2-7. Calibration curve of 5,7-DMF in mouse intestine.

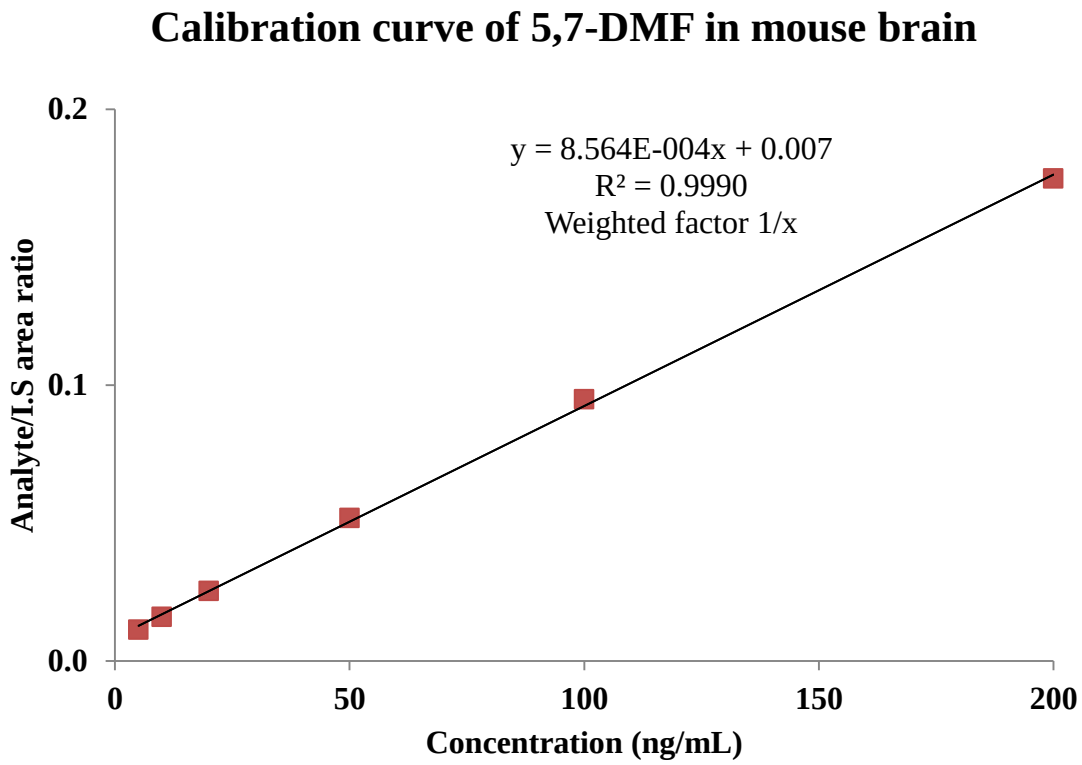

Figure 2-8. Calibration curve of 5,7-DMF in mouse brain.

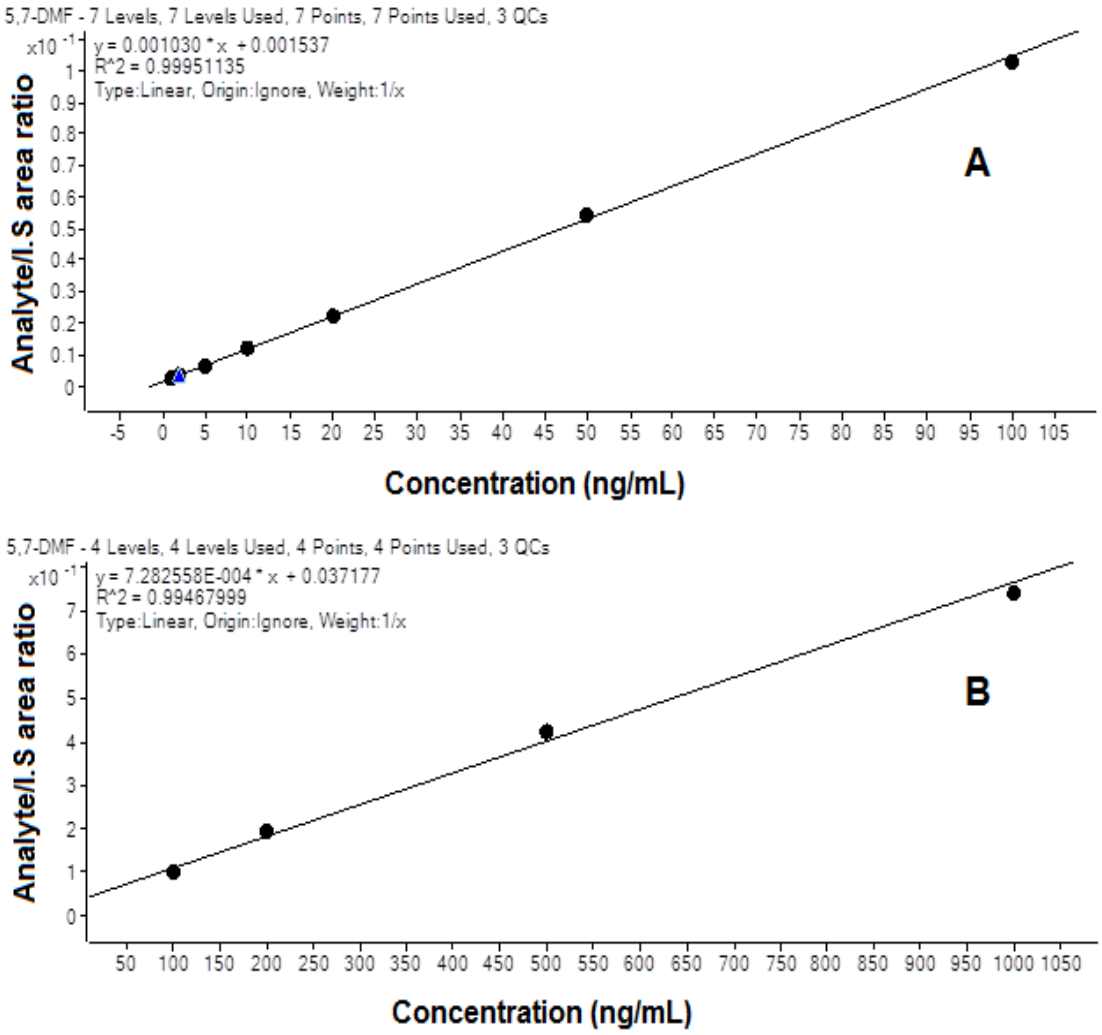

Figure 2-9. Calibration curve of 5,7-DMF in mouse spleen.

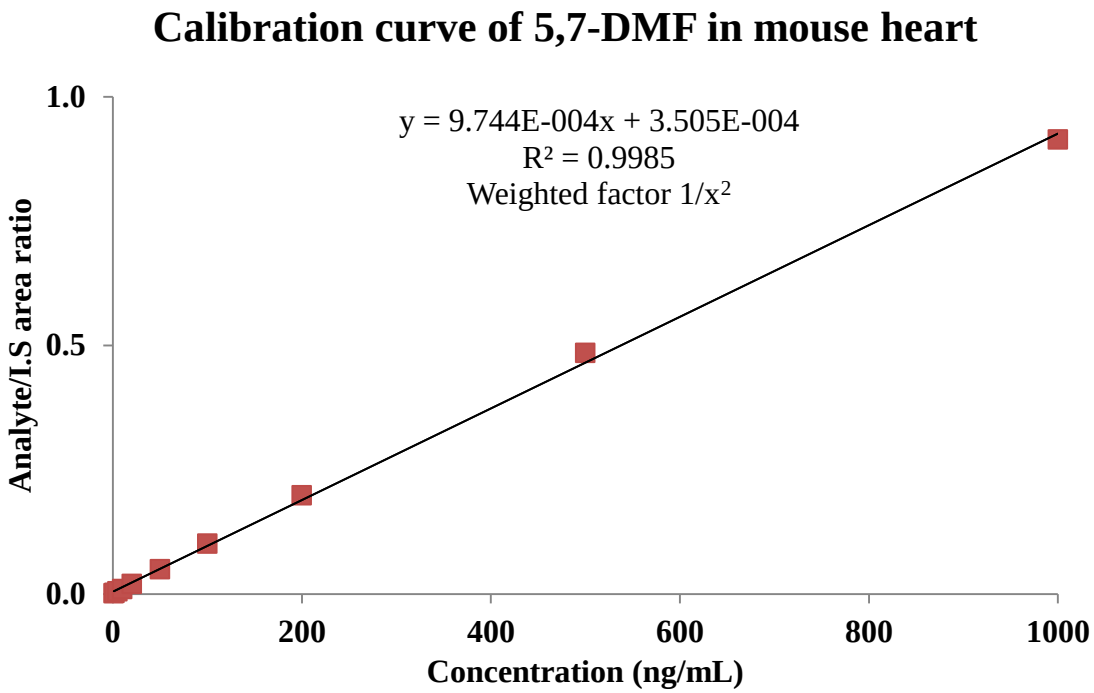

Figure 2-10. Calibration curve of 5,7-DMF in mouse heart.

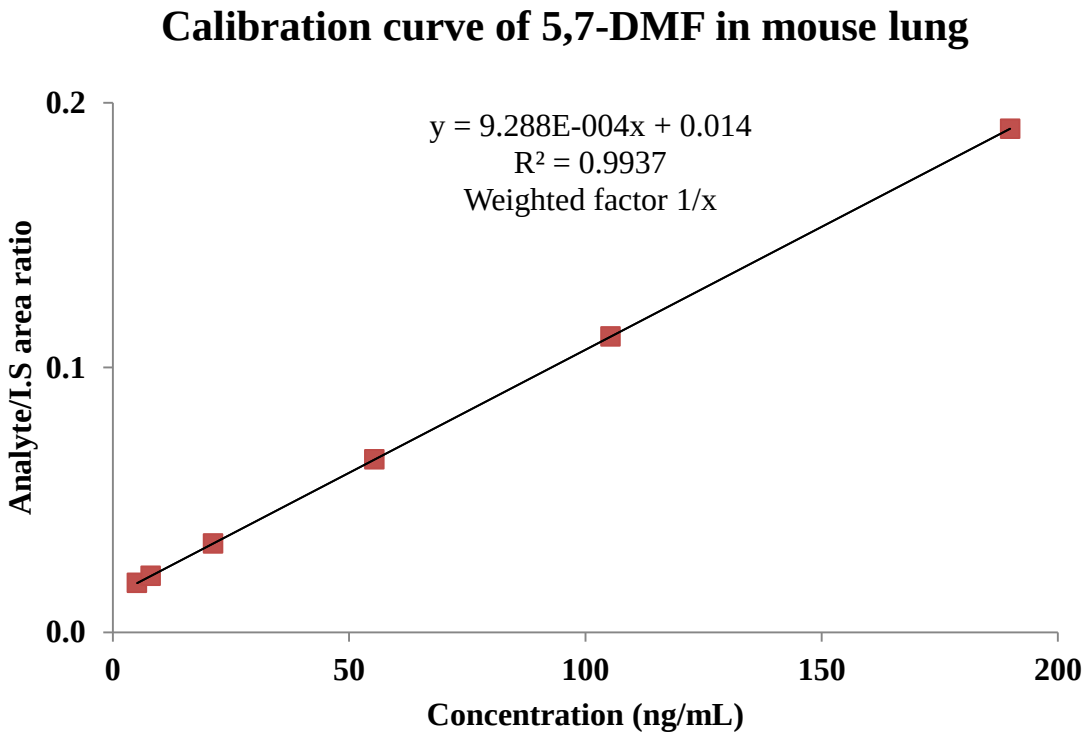

Figure 2-11. Calibration curve of 5,7-DMF in mouse lung.

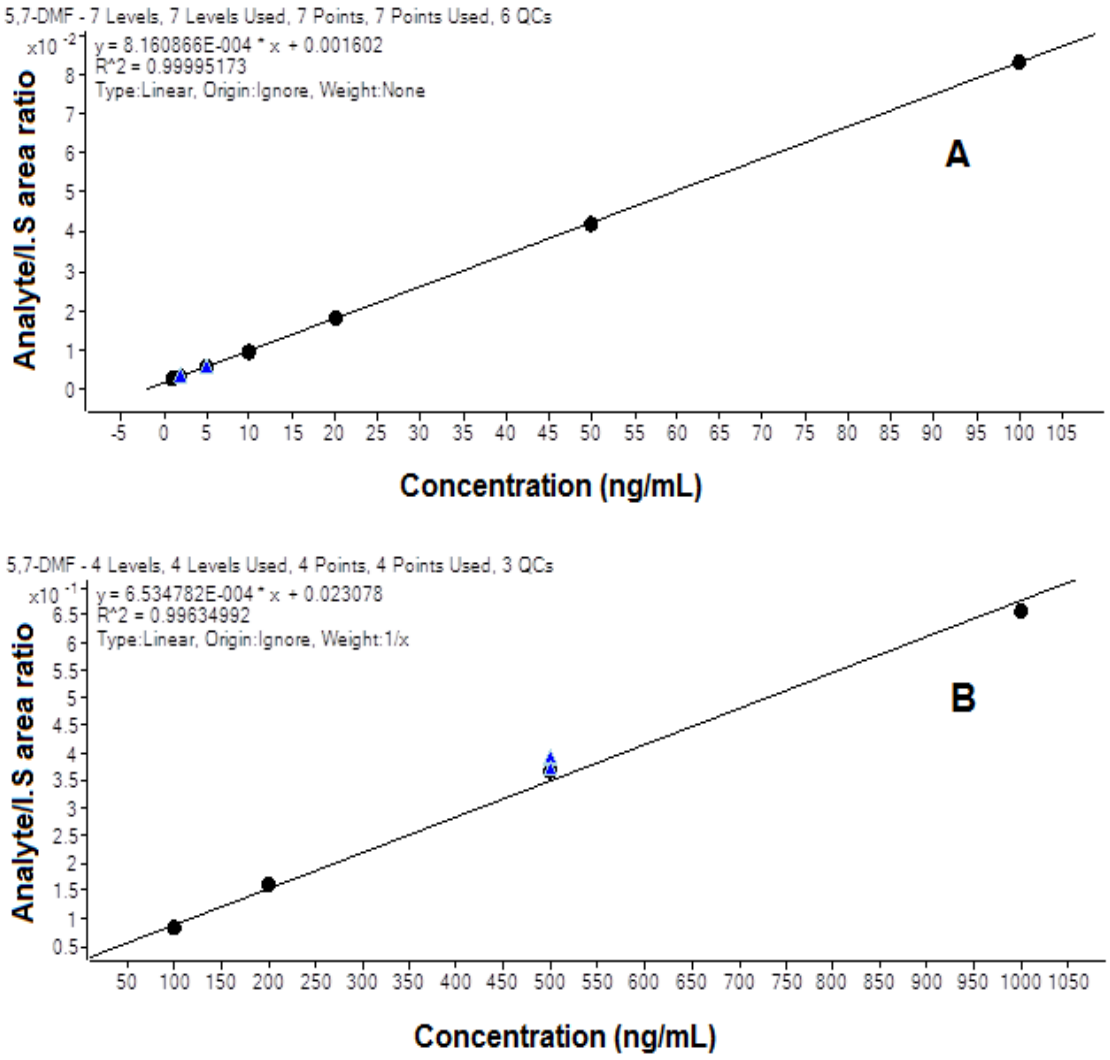

Figure 2-12. Calibration curve of 5,7-DMF in mouse muscle.

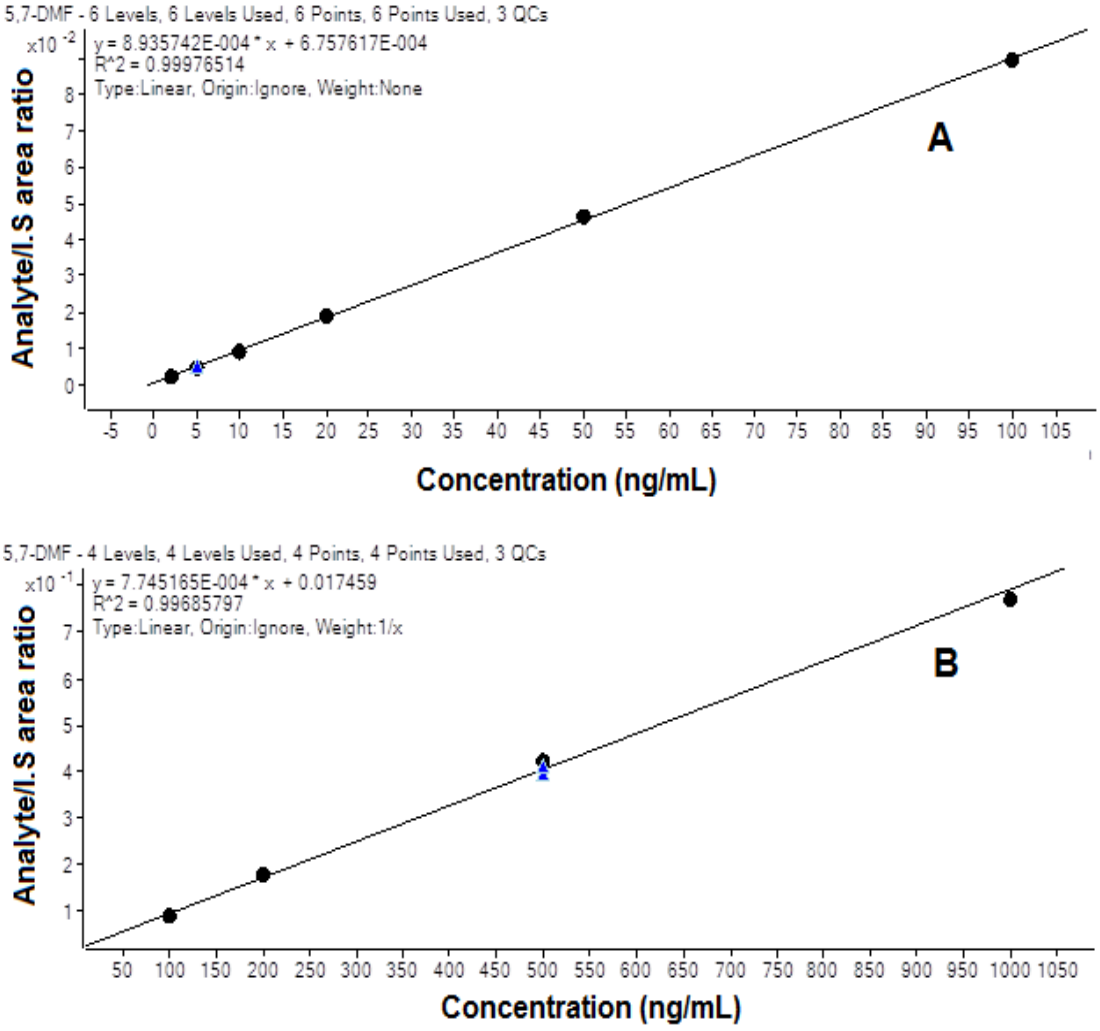

Figure 2-13. Calibration curve of 5,7-DMF in mouse fat.

Table 2-8. Method validations of 5,7-DMF in mouse plasma and tissues (N=3).

Tissue	Conc. (ng/mL)	Mean conc. (ng/mL)	Accuracy (%)	CV (%)
Plasma	2	2.18	109	3.54
	500	552	110	0.92
Liver	2	1.84	92.2	6.17
	500	525	105	1.50
Kidney	2	2.18	109	3.30
	500	536	107	1.58
Brain	2	1.96	98.1	1.70
	500	528	106	5.10
Intestine	2	1.95	97.5	12.3
	500	506	101	2.37
Spleen	2	1.92	95.8	3.10
	500	460	92.0	*
Heart	2	1.97	98.5	6.59
	500	552	111	2.75
Lung	2	2.13	107	19.6
	500	555	111	2.28
Muscle	2	2.29	115	3.05
	500	554	111	2.79
Fat	2	4.93	98.7	1.56
	500	496	99.1	2.06

(*denotes one determination)

Discussions

Compared to two assays on 5,7-DMF published in the past [44, 48] , our assay is simpler and more sensitive. Sutthanut et al. reported a LLOQ of 5,7-DMF at 800 ng/mL using GC, whereas Mekjaruskul et al. reported a LLOQ of 5,7-DMF at 1.86 μg/mL using HPLC-UV. Our result of LLOQ of 2 ng/mL demonstrates to be a significant improvement in the assay sensitivity, which is useful in quantification in terminal phase of plasma samples. Furthermore, in terms of sample preparation, our study used ethyl acetate to extract sample only once, compared to Mekjaruskul's method of using ethyl acetate three times to extract analytes. In addition, our assay is much faster than the other two assays since the retention time for 5,7-DMF in our assay is 3.7 min compared with 9 min and 26 min for GC method and HPLC method, respectively. Our quantification methods in mouse plasma can be applied in clinical trials and adapted to measure 5,7-DMF concentration in human plasma and human liver, kidney, brain, intestine, spleen, heart, lung, muscle and fat tissues as well.

One interesting finding about the matrix effect was that, in matrix blank such as blank mouse plasma, and other mouse tissues, there seemed to exist ‘ghost peak’. Supposedly, the matrix blank didn’t have any analyte. However, as shown in Fig. 2-3 A, the small ‘bump’ exhibited in blank mouse plasma was not due to error or contamination in the samples. It was constantly showing up in the XIC which could negatively affect the LLOQ. But it was observed that with increase in the analyte concentration, the noise signal didn’t increase proportionally. But even with the strongest cleaning organic solvents, it couldn’t get rid of such noise signal. It may be because of trace amount of analyte getting stuck inside certain part of the column due to the physic-chemical interaction between the chemical and the column stuff. More often than not, such

interference appeared in LC-MS/MS. The bottom line is to ensure such signal-to-noise ratio is greater than 5. And in our case, the LLOQ of 2 ng/mL had a signal-to-noise ratio of above 7. So the ghost peak wouldn’t affect quantification for concentrations larger than that.

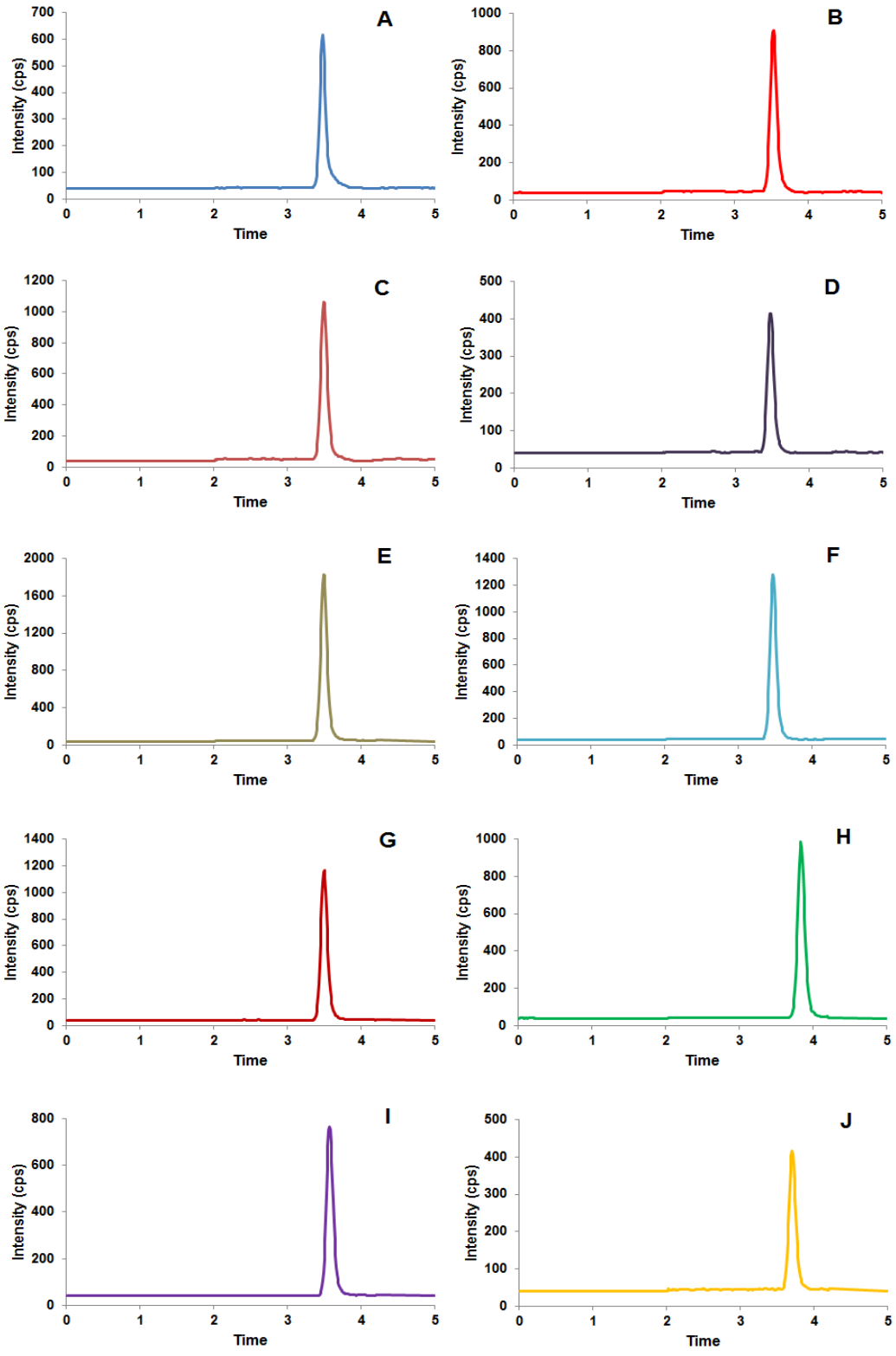

Figure 2-14. XIC of the 5,7-DMF and I.S in mouse plasma and tissues

Table 2-9. Comparison among different sample preparation methods on quantification of liver samples from a pilot study.

Method	Sample ID	Measured conc. (ng/mL)
A	2h-1	4.75
	2h-2	14.7
	2h-3	21.8
B	2h-1	6.13
	2h-2	13.8
	2h-3	17.0
C	2h-1	5.90
	2h-2	12.9
	2h-3	16.5
D	2h-1	5.18
	2h-2	17.1
	2h-3	25.8

Summary

A fast, accurate, sensitive and selective quantification method of DMF was established to warrant further PK study in mice. The LLOQ of this method is 2 ng/mL. This quantification method was validated and the matrix effect and recovery yield were consistent and reproducible. The stability of 5,7-DMF in stock solution, in −80 °C freezer for up to 2 weeks and the stability in up to three freeze–thaw cycles were also proved. The developed method was successfully adapted to and validated on mouse tissues, including liver, kidney, heart, lung, spleen, brain, intestine, muscle and fat. This warrants further PK study of 5,7-DMF in mice.

CHAPTER 3
PHARMACOKINETICS AND TISSUE DISTRIBUTION OF 5,7-DMF IN MICE

Background

5,7-DMF has been evaluated extensively in vitro and the results showed that 5,7-DMF has many beneficial pharmacological activities. For example, it has anti-inflammatory activity [30], vasorelaxation and cardioprotection effect by increasing potassium efflux and inhibiting calcium influx [31], and selectively inhibitory effect against butyrylcholinesterase versus acetylcholinesterase [32]. Moreover, Walle's group conducted a series of in vitro studies to evaluate the chemotherapeutic and chemopreventive potential of this compound [33-35]. They found that 5,7-DMF can prevent hepatic carcinogenesis by inhibiting Cytochrome P450 (CYP) 1A1 activity, which subsequently decreased the carcinogenbenzo[a]pyrene (BaP)-induced DNA adduct formation [35].

The chemopreventive effect of 5,7-DMF was also observed in human esophageal cancer cells and human oral carcinoma cells by regulating CYP1B1 activity [34-35]. 5,7-DMF was also reported to have chemosensitizing effect in hetapocellular carcinoma cells and human leukemic cells through tumor necrosis factor-related apoptosis-inducing ligand (TRAIL)-mediated apoptosis [36-37]. In addition, 5,7-DMF was shown to improve the accumulation of rhodamine 123 into the cells with overexpression of P-glycoprotein (P-gp), an efflux transporter which is present in various cancer cells and plays an important role in multi-drug resistance (MDR) [27]. In addition to P-gp inhibition, 5,7-DMF also has inhibitory effect on other two efflux transporter members - multidrug resistance associated-proteins (MRPs) and Breast Cancer Resistance Protein (BCRP).

It is noteworthy however, that most of the literature reported the beneficial efficacy of 5,7-DMF in vitro, but the report on its in vivo PK profile is very limited. Currently, there is one paper reporting PK in killifish, and two papers reporting PK in rats. The PK in mice and other animal species are still missing. Therefore, in this chapter, we will explore the PK of 5,7-DMF in mice to study its dose proportionality, bioavailability and tissue distribution. Previously, the analytical methods available can only quantify 5,7-DMF with the lower limit of quantification (LLOQ) of more than 800 ng/mL [44,48]. In our recent study, we established a fast, accurate and sensitive LC-MS/MS method to quantify 5,7-DMF in mouse plasma with the LLOQ of 2 ng/mL [55]. It was applied to this study to investigate the PK profile and tissue distribution of 5,7-DMF in mice in this chapter.

Material and Methods

Chemicals and Reagents

5,7-DMF (>99%,) and 5,7,4'-trimethoxyflavone (TMF, >99%), shown in Fig 1 were purchased from Indofine Chemical Company, Inc (Hillsborough, New Jersey, US). Ammonium formate (99%) was obtained from ACROS Organics (New Jersey, US). Analytical HPLC grade acetonitrile (ACN), isopropanol, water, ethanol, phosphate-buffered saline (PBS) 10X solution, Triton lysis buffer (pH 8.0) and formic acid were purchased Fisher Scientific (Pittsburg, Pennsylvania, US). Analytical spectrophotometric grade ethyl acetate (99.5%) was obtained from Alfa Aesar (Ward Hill, Massachusetts, US). Cyclohexane Hexahydrobenzene (99.5%) was purchased in VWR International LLC (Philadelphia, Pennsylvania, US). Heparin-treated mouse plasma was purchased from BioreclamationIVT (East Meadow, New York, US). Poly(ethylene glycol) Mn 400 (PEG400) were purchased through Sigma Aldrich (St. Louis, Missouri, US). Heparin

Injectable (1,000 U/mL) was purchased from Patterson Vet Generics (Devens, Massachusetts, US). Isoflurane was provided in Animal Facility surgery room under IACUC protocol.

Animals and In-Vivo Study

4-6 weeks old Harlan's ND4 male Swiss Webster mice with the average body weight of 26.2 g were obtained from Harlan Laboratories. Before experiment, all mice were settled and housed in the University of Florida (UF) Animal Research Facility for a week following a 12 hr light/dark cycle. All mice had access to normal/standard diet and water and this in vivo study was carried out in accordance with IACUC protocol evaluated and approved by review board of UF Animal Care and National Institutes of Health.

In dose linearity study, 90 mice were randomly separated into 3 dosing groups with each group of 30 mice assigned randomly into 10 time points (up to 48 h) triplicate mice at each time point (N=3). 10, 25 or 50 mg/kg 5,7-DMF was administered through penile vein injection (IV) to the mice. The mice had free access to food and water before and after oral administration. Mouse plasma was collected after immediately centrifuged at 2,000 g. Supernatant layer of the blood was thus collected as plasma and all the plasma and tissue samples were stored at -80ºC until analysis.

In bioavailability study, 60 mice were randomly separated into either IV or Oral group with each group of 30 mice assigned randomly into 10 time points triplicate mice at each time point (N=3). 5,7-DMF was first dissolved in dimethyl sulfoxide at the concentration of 20 mg/mL and prior to dosing, it was further diluted as solution in the vehicle consist of 35% PEG400, 2% ethanol and 63% deionized water at the final concentration of 2 mg/mL. This solution containing 2 mg/mL 5.7-DMF was stable in the

vehicle for at least 24 hr under room temperature. The target dose of 10 mg/kg 5,7-DMF was administered through either penile vein injection (IV) or through oral gavage to the mice. The mice had free access to food and water before and after oral administration. Blood, heart, lung, gut, brain, liver, kidney, spleen, muscle and adipose tissues were collected at time points 5, 15 and 30 min and 1, 2, 3, 4, 8, 12 and 21 hr after oral dosing. Mice were euthanized by isoflurane followed by cervical dislocation. The heparinized blood was immediately centrifuged at 2,000 g for 8 min with a mini-centrifuge. Supernatant layer of the blood was thus collected as plasma and all the plasma and tissue samples were stored at -80ºC until analysis.

Sample Preparations and LC-MS/MS Assays

The LC-MS/MS condition was the same as previously reported [20]. Briefly, under positive mode of Agilent triple quadruple 6460, 5,7-DMF (m/z 283 > m/z 239) and I.S (m/z 313 > m/z 298) were simultaneously monitored with isocratic elution at a flow rate of 0.4 mL/min. The mobile phase is 50/50 (v/v) of 20 mM ammonium formate in water and acetonitrile. Plasma sample preparation method was completed following previous reported method [55]. For tissue samples, tissue was weighed and added PBS buffer (pH=7.4) based on 10-fold volume of each tissue weight. They were cut into smaller pieces before homogenization. Then 10 µL of I.S was spiked into 100 µL of tissue homogenate. Other steps were the same as plasma sample preparation. After vortex mixing for 1 min, 600 µL of ethyl acetate was added for liquid-liquid extraction on a mechanical shaker for 5 min. Then the supernatant layer was transferred to clean tubes after the centrifuge at 17,000 rpm under 4 ºC for 4 min, and placed under nitrogen for evaporation. The residue was reconstituted with 100 µL of mobile phase and centrifuged at 17,000 rpm under 4 ºC for 4 min to get rid of precipitation. 5 µL of the

supernatant aliquot was injected to the LC-MS/MS. Calibration curve were prepared at concentrations 2, 5, 10, 20, 50, 100, 200, 500 and 1000 ng/mL in blank mouse tissues.

Pharmacokinetic Analysis

The non-compartmental analysis (NCA) was employed to calculate the PK parameters using Phoenix 1.3 (Pharsight, Mountain View, CA). Lambda z (λ_z) is the elimination rate constant at the terminal phase, and it was calculated as the slope of the linear regression on the terminal data points. C_{max} is the maximal plasma concentration based on the experimental data. The area under the plasma concentration time curve from time zero to the last time point (AUC_t) was calculated by linear trapezoidal rule. AUC infinity (AUC_{inf}) was determined by AUCt plus extrapolated portion C_t/λ_z. Terminal half-life was calculated as 0.693/λz. The systemic clearance (CL_F) was determined as Dose/AUC_{inf}. The apparent volume of distribution (V_z_F) was calculated as CL_F/λ_z. The partition coefficient in tissue (K_p) was calculated by AUC_t (area under the curve from 0 to the last time point that the analyte can be measured) of tissue divided by AUC_t of plasma.

Results

LC-MS/MS Method Development and Validation

As reported, our LC-MS/MS quantification method on mouse plasma was proven to be accurate, reliable, fast, sensitive and selective [55]. It was fully validated and the precision and accuracy of various QC samples all passed the criteria based on FDA guideline [c]. In this study, it was applied and validated in tissue matrices. As indicated by the FDA guideline and the newest draft guidance [54, 56], the change in the biological matrices within same species is the typical method modification and only partial validation is needed. Further, it is indicated in these guidance that, the total

number of QC samples should be either 5% of the total samples to be analyzed or at least 6 QC samples in total, whichever number is greater [54, 56]. Therefore, in this case, for each tissue analysis, we performed intra-day validations on various concentrations with each concentration in triplicates (N=3) and the method validation results were shown in Table 2-8. Our results indicated QC samples at LLOQ were within 20% of the nominal concentrations and QC samples at higher concentrations were within 15% of the nominal concentrations. Thus these quantification methods were successfully validated and sample analyses using these assays were reliable. The XIC of 5,7-DMF in tissue samples were shown in Fig 2-14.

The sample preparation method for tissue samples was optimized based on the comparison of four tissue preparation methods from a pilot study. Among these four methods, the measured extraction efficiency was the highest in method D. The detailed comparison of these four extraction methods was listed in Table 2-9. Method D exhibited constant higher extraction efficiency for different sample ID. Besides, the procedures of method D were relatively simple and less time consuming. Due to the simple and efficient procedure of method D, it was applied for tissue preparations in this study.

Dose Linearity of 5,7-DMF in Mice

5,7-dmf solution within the dosing range of 10 to 50 mg/kg resulted in linear PK profile, as shown in Fig 3-1. Time courses of 10-50 mg/kg administration were almost parallel to each other. The NCA parameters were listed in Table 3-1. The area under the curve (AUCinf) and peak plasma concentration (Cmax) of each dose was proportional with dose.

Table 3-1. Dose linearity of 10-50 mg/kg IV dose in mice (N=3).

Parameter	10mg/kg	25mg/kg	50mg/kg
C_{max} (ng/mL)	8823 ± 1516	23384 ± 1422	44867 ± 11137
AUC_{inf} (h*ng/mL)	3292 ± 1042	10659 ± 647	20039 ± 1424
CL (L/h/kg)	3.25 ± 1.04	2.35 ± 0.14	2.50 ± 0.18

Bioavailability of 5,7-DMF in Mice

When compared the NCA results between IV and oral dose of 10 mg/kg 5,7-DMF solution, as shown in Table 3-2, the mean AUC of IV and oral routes were 3886 and 537, respectively, which made the calculated bioavailability at 13.8%, based on the equation $F = \frac{Dose_{iv} \times AUC_{po}}{Dose_{po} \times AUC_{iv}} \times 100\%$, where AUC_{po} is the AUC after oral dose and AUC_{iv} is the AUC after IV dose.

The time course of both dosing routes was shown in Fig. 3-2. The curve shape at the terminal phase seemed similar. There was no sign of flip-flop phenomenon. The oral absorption was fast. The IV dosing route, plasma concentration was detectable up to 4 h while in oral route, the plasma concentration was detectable up to 12 h.

Table 3-2. Bioavailability of 5,7-DMF following 10 mg/kg IV and oral dose (N=3).

Parameter	IV dose	Oral dose
AUC_{inf} (h*ng/mL)	3886 ± 222	537 ± 167
Bioavailability%	-	13.8
CL (L/h/kg)	2.58 ± 0.15	20.6 ± 7.49
C_{max} (ng/mL)	8119 ± 2180	1868 ± 1194
$T_{1/2}$ (h)	0.68 ± 0.32	3.4 ± 2.8
V_F (L/kg)	2.52 ± 1.20	90.1 ± 62.0

Pharmacokinetic Analysis and Tissue Distribution in Mice

The NCA result in Table 3-3 showed that the maximal plasma concentration following oral dose of 10 mg/kg 5,7-DMF was 1870 ± 1190 ng/mL. The terminal half-life $t_{1/2}$ was 3.40 ± 2.80 hr. The volume of distribution by the area method V_z_F was 90.1 ±

62.0 L/kg. Clearance (CL_F) was 20.2 ± 7.49 L/hr/kg. The drug exposure AUC_t and AUC_{inf} was 532 ± 165 and 537 ± 167 hr*ng/mL, respectively.

Table 3-3. Non-compartmental parameters of 5,7-DMF in mouse plasma after oral administration of 10 mg/kg 5,7-DMF (N=3). The data were presented as mean and standard deviation.

Parameter	Estimate
λ_z (1/hr)	0.30 ± 0.17
C_{max} (ng/mL)	1870 ± 1190
T_{max} (hr)	0.14 ± 0.10
AUC_t (hr*ng/mL)	532 ± 165
AUC_{inf} (hr*ng/mL)	537 ± 167
$T_{1/2}$ (hr)	3.40 ± 2.80
CL_F (L/hr/kg)	20.2 ± 7.49
V_z_F (L/kg)	90.1 ± 62.0

The concentration-time profiles of plasma, liver, kidney, gut and brain were presented in Fig. 3-3. Through the oral gavage, the C_{max} of 5,7-DMF was quickly reached among plasma and tissues within 0.5 hr after dosing due to fast absorption, with mean T_{max} ranging from 0.14 to 0.36 hr. The semi-log scale plots indicated a bi-exponential disposition pattern of 5,7-DMF. The plasma concentration after T_{max} dropped drastically due to fast and vast distribution into tissues and then it followed a long terminal phase probably because of the contribution of the 5,7-DMF in the tissue back to plasma. The analyte was detectable up to 21 hr in mouse plasma, gut, liver, kidney, spleen and adipose. The time-course of mouse liver, kidney, gut, spleen and adipose followed the same pattern as that of mouse plasma.

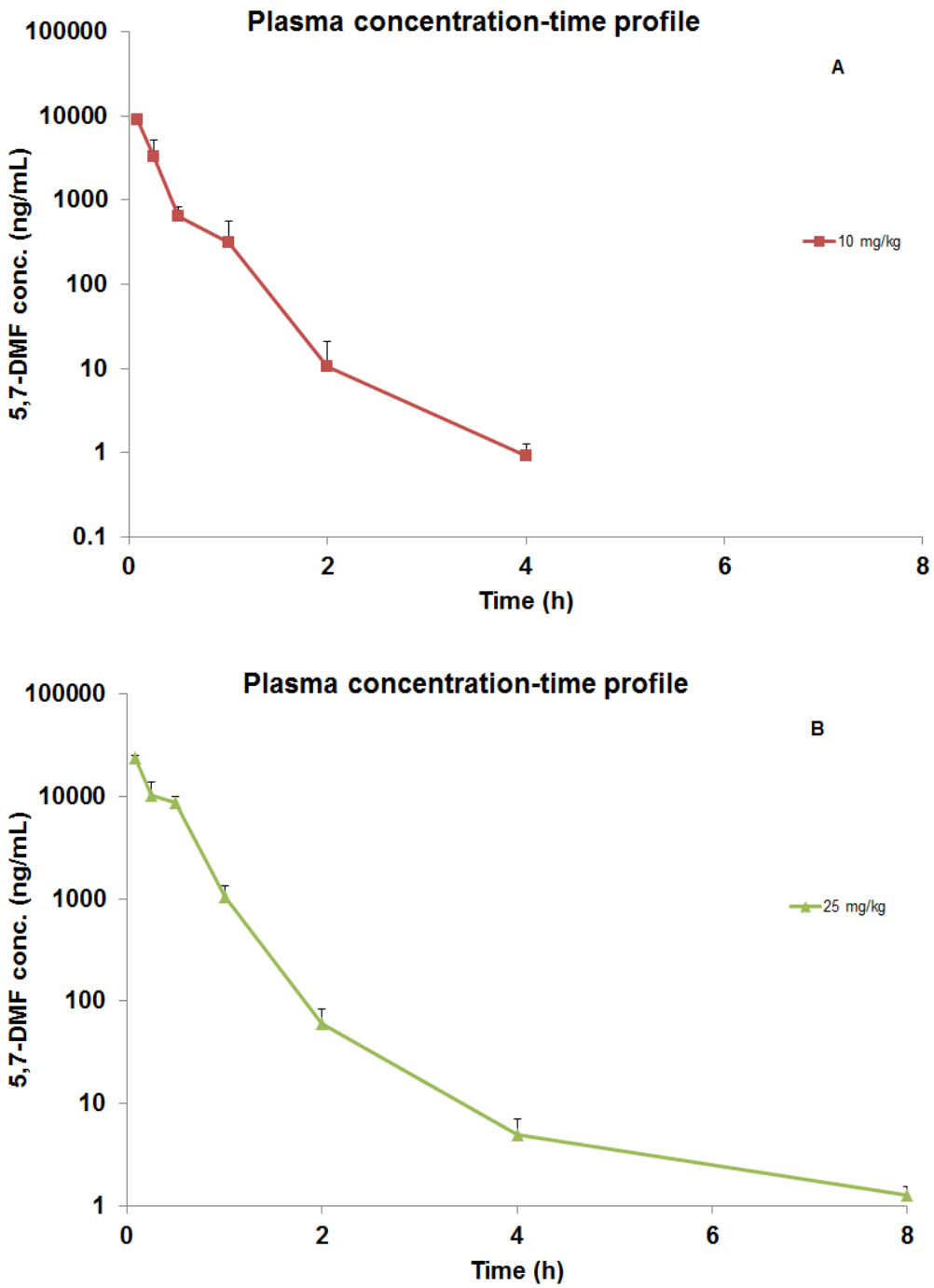

Figure 3-1. Dose proportionality in mice. Plasma PK profile (mean±SD) of 10 (A), 25 (B) and 50 (C) mg/kg IV dose of 5,7-DMF(N=3).

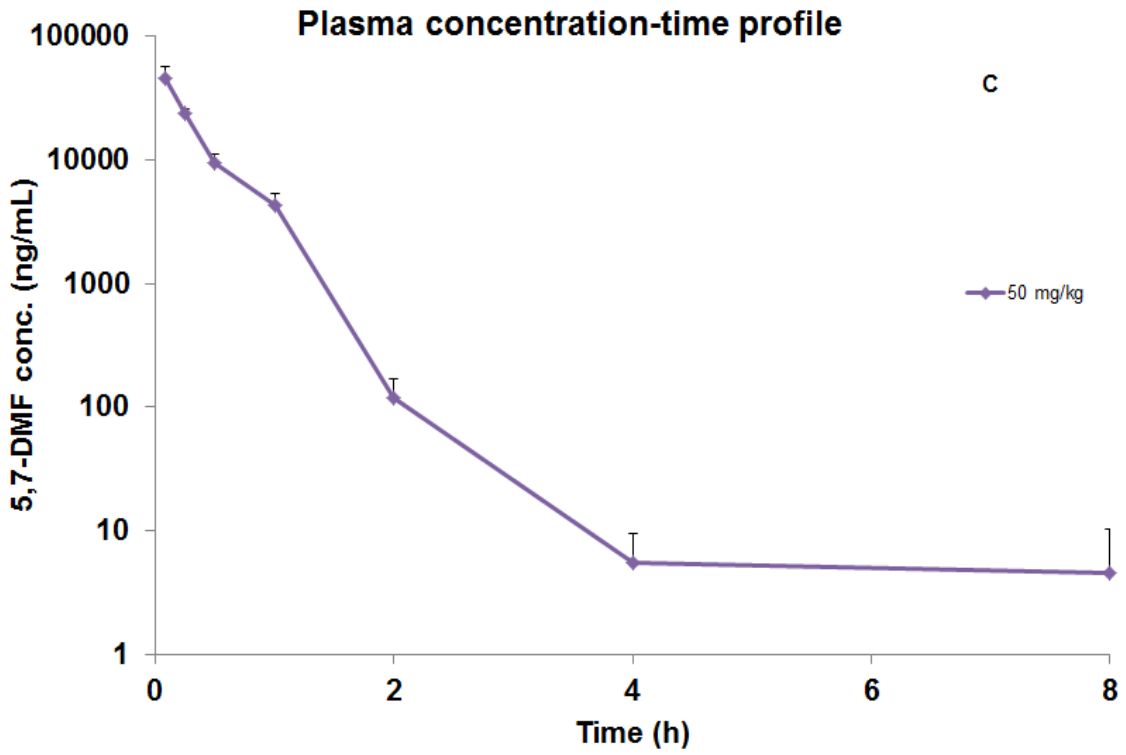

Figure 3-1. Continued.

As shown in Fig. 3-4, the 5,7-DMF concentration in mouse tissues were much higher than that in mouse plasma. Except for muscle and adipose, other tissues had the C_{max} higher than that in the plasma, ranging from 1.75- to 9.96-fold. The highest tissue C_{max} was in mouse gut, followed by liver, brain, kidney, heart, spleen, lung, muscle and adipose. As indicated by the NCA analysis results listed in Table 3-4, AUC_t of gut, liver, kidney, brain and spleen were 6850 ± 1360, 4640 ± 518, 2100 ± 667, 1520 ± 554 and 1250 ± 82 hr*ng/g, respectively. Thus, 5,7-DMF exposure in these tissues were 2.35- to 12.9-fold higher than that of mouse plasma. It is shown that 5,7-DMF through oral dose was most abundant in gut, followed by liver, kidney, brain, spleen, heart, lung, adipose and lastly, muscle.

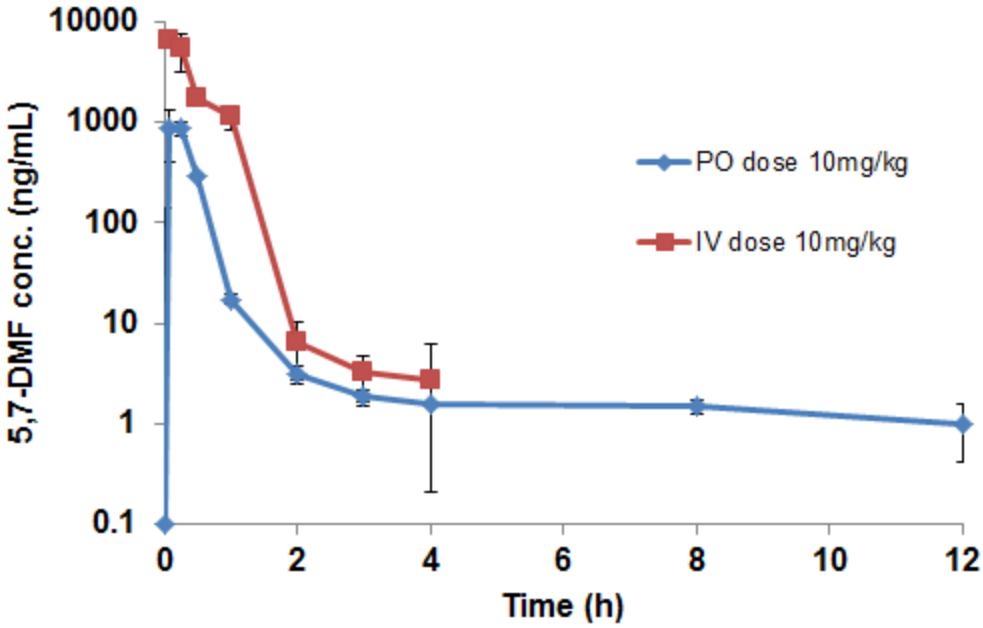

Figure 3-2. Plasma PK profile (mean±SD) of IV and oral dose of 10 mg/kg 5,7-DMF in mice (N=3).

Table 3-4. PK parameters of 5,7-DMF in mouse tissues after oral administration of 10 mg/kg 5,7-DMF (N=3). The data were presented as mean and standard deviation.

Parameter	C_{max} (ng/g)	AUC_t (hr*ng/g)	K_p
Intestine	18600 ± 4290	6850 ± 1360	12.9
Liver	10900 ± 3140	4640 ± 518	8.71
Kidney	7200 ± 5820	2100 ± 667	3.94
Brain	7260 ± 5740	1520 ± 554	2.86
Spleen	3260 ± 2200	1250 ± 82	2.35
Heart	4990 ± 4220	1230 ± 355	2.31
Lung	3030 ± 1450	781 ± 148	1.47
Fat	558 ± 290	529 ± 293	0.99
Muscle	1180 ± 739	345 ± 110	0.65

The PK profile of plasma and nine other tissues was shown in Fig. 3-4. The calculated K_p values for major tissues were listed in Table 3-4. K_p values for intestine,

liver, kidney, brain, spleen, heart, lung, fat and muscle were 12.9, 8.71, 3.94, 2.86, 2.35, 2.31, 1.47, 0.99 and 0.65, respectively. They will be further evaluated in our future investigation on the physiologically based PK modeling of 5,7-DMF.

Discussions

Breast Cancer Resistance Protein (BCRP) is one of the main efflux transporters associated with MDR. 5,7-DMF has been reported to be a potent inhibitor of BCRP, with an IC_{50} of 2.5 μM (equivalent to 0.703 μg/mL) [39-40]. 5,7-DMF can significantly increase the accumulation of mitoxatrone (an anticancer agent) in BCRP-overexpressed breast cancer cells and correspondingly enhanced the cytotoxicity of mitoxatrone in those cells at nano-molar to low micro-molar concentration range. In this case, under the dose of our study (10 mg/kg), 5,7-DMF plasma level of 2.5 μM could be reached, which can effectively inhibit BCRP at the cellular level and may represent clinical relevance in cancer treatment.

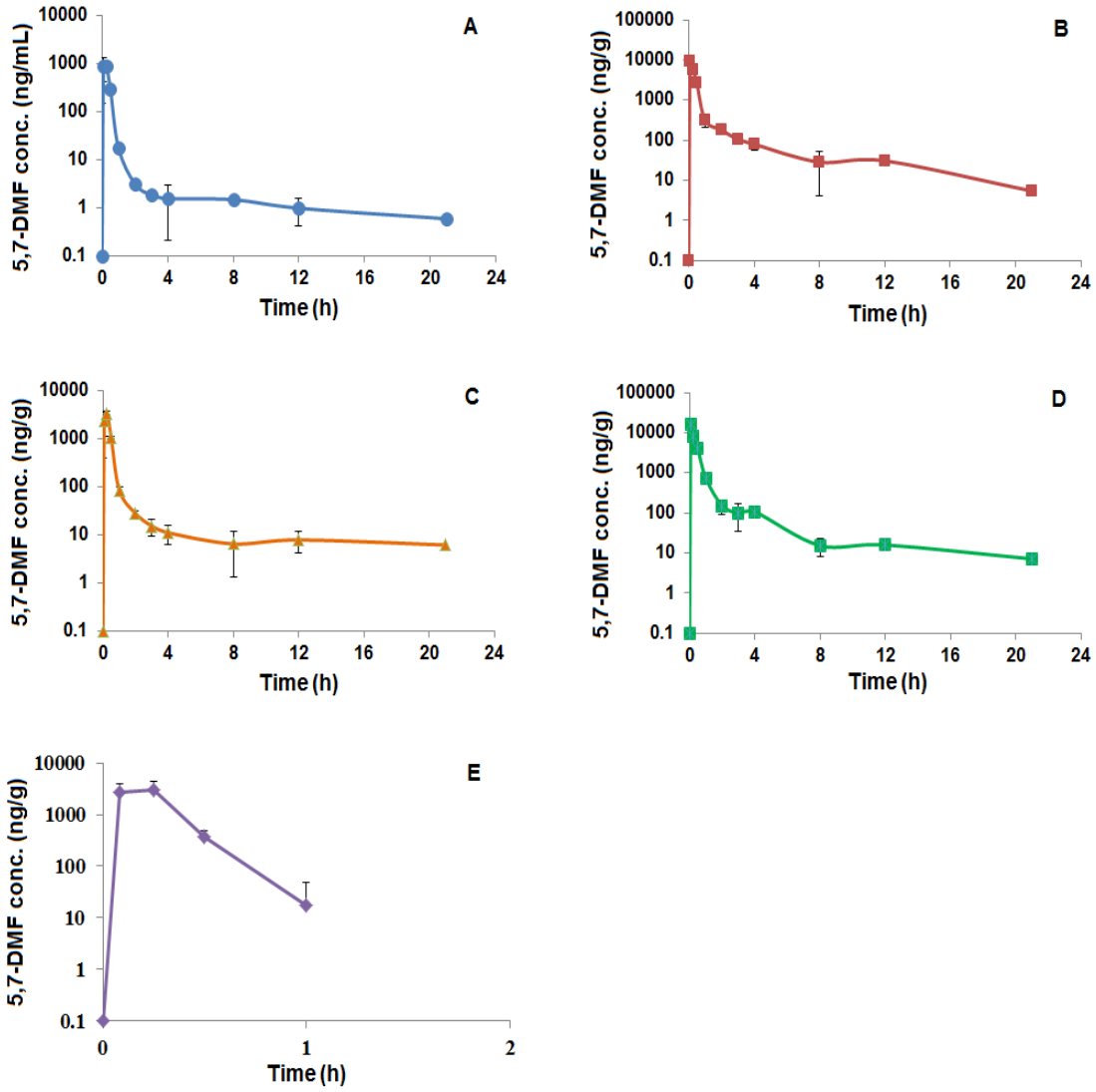

Figure 3-3. Concentration-time profiles of 5,7-DMF in mice following oral administration of 10 mg/kg 5,7-DMF (N=3). A, B, C, D and E represented the pharmacokinetic profile of 5,7-DMF in mouse plasma, liver, kidney, small intestine and brain.

The pharmacokinetic parameters of 5,7-DMF after 10 mg/kg oral dose in mice were determined in this study. Based on the previous literature, 10 and 30 mg /kg equivalent 5,7-DMF oral doses were proven safe in rats [44]. In addition to 10 mg/kg oral dose, we also evaluated 10, 25 and 50 mg/kg intravenous dose in our pilot study and no toxicity was observed at any dose tested, indicating the favorable safety profile of 5,7-DMF. In addition, our pilot study had demonstrated the linear relationship between dose and concentration on 10, 25 and 50 mg/kg intravenous dose of 5,7-DMF. Therefore the C_{max} and AUC can be reasonably estimated within that dosing range.

It has been reported that the IC_{50} value of 5,7-DMF for BCRP inhibition in vitro is 1.41 μM and at this concentration 5,7-DMF can significantly increase the intracellular accumulation of mitoxantrone in the BCRP-overexpressing cells [39-40]. Our result revealed that under 10 mg/kg oral dose, 5,7-DMF could easily reach the concentration of 1.41 μM (equivalent to 398 ng/mL) in plasma and various tissues. Based on our results, it is reasonably to speculate that the BCRP inhibitory effect of 5,7-DMF observed in vitro can be extrapolated to in vivo. Similarly, 5,7-DMF was reported to increase the doxorubicin accumulation into P-gp overexpressed cell-line in a concentration-dependent manner within 1-300 μM (282-84600 ng/mL) [27], and this in vitro P-gp inhibitor effect should be able to be translated to in vivo as well since our PK data showed that the C_{max} of 5,7-DMF in plasma and different tissues range from 1870 to 18600 ng/ml (Tables 3-1 and 3-2).

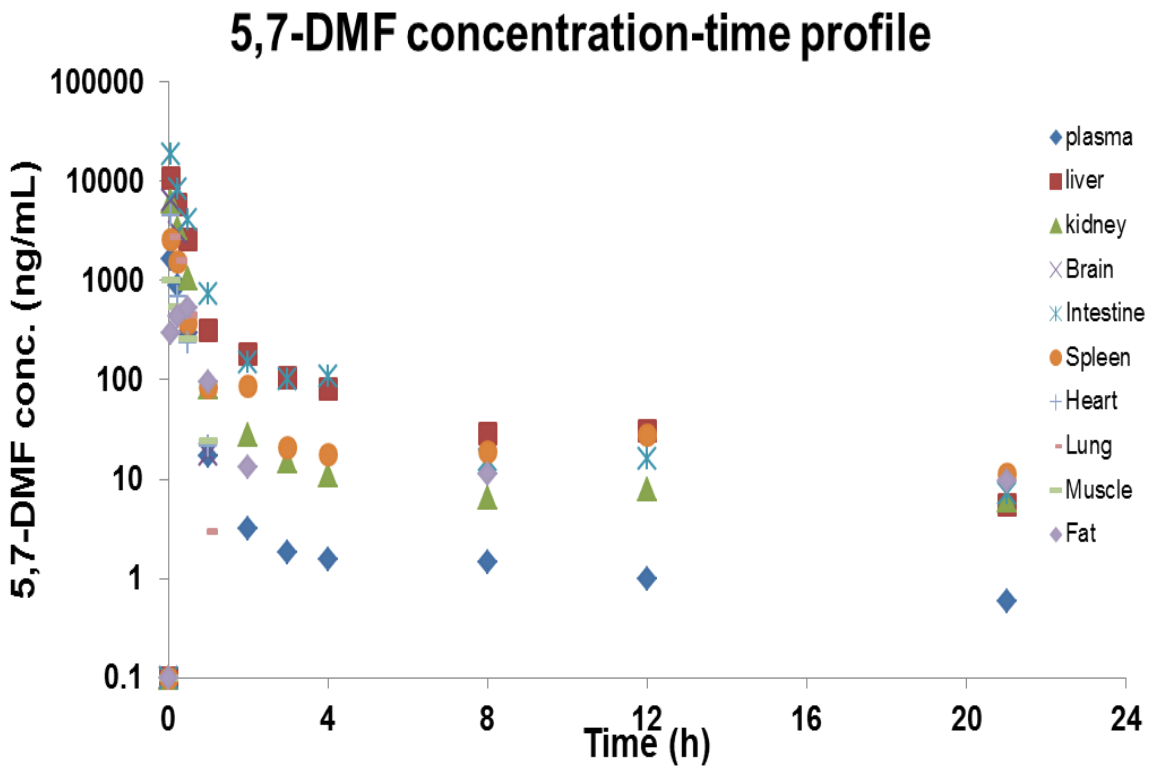

Figure 3-4. Mean plasma and tissue PK profiles of oral dose of 10 mg/kg 5,7-DMF in mice (N=3).

Terminal half-life of 5,7-DMF calculated in plasma was 3.40 ± 2.80 hr, so it might take 17 hr (5 half-lives) to clear 5,7-DMF completely (>95%). T_{max} for mouse gut, plasma, liver and kidney were 0.083 ± 0.00, 0.14 ± 0.10, 0.14 ± 0.10 and 0.19 ± 0.10 hr, respectively, indicating rapid distribution of the 5,7-DMF from plasma to tissues [44]. The peak concentration in major tissues such as liver, brain, kidney, heart, and lung were higher than plasma peak concentration, with the C_{max} ratio to plasma of 5.86, 3.88, 3.85, 2.67 and 1.62, respectively. The high tissue accumulation was also in accordance with Walle's paper, in which maximal liver concentration of 5,7-DMF was 7-fold higher than that of plasma level and the peak lung and kidney 5,7-DMF were almost 2-fold higher than plasma concentration [44].

The large value of volume of distribution indicated extensive accumulation in tissues, which was consistent with observations in Mekjaruskul's and Walle's studies [43-44]. This may indicate tissues as the favorable sites for 5,7-DMF to exert the greatest pharmacological action. Among different studies and different species, 5,7-DMF may have different tissue distribution profile. In our study, we found that in mice, the compound after oral dosing was most concentrated in gut > liver > spleen > kidney > brain > heart > lung> adipose > plasma > muscle. And Walle's paper reported 5,7-DMF most accumulated in rats liver > lung > kidney > plasma [44] whereas Mekjaruskul's paper reported rats concentration liver > plasma > kidney > lung [43]. 5,7-DMF in killifish was reported to have highest concentration in liver > brain > gut > gill > skin [48]. But in general, liver and kidney had higher 5,7-DMF than other tissues and plasma probably because they are well-perfused organs. It is noteworthy that liver was the major tissue for 5,7-DMF accumulation. 2-20 μM (564-5640 ng/mL) of 5,7-DMF was achievable through this 10 mg/kg oral dose which was reported to inhibit benzo[a]pyrene-induced DNA binding in liver [33]. Also, 2.5-10 μM (705-2820 ng/mL) of 5,7-DMF was achievable in vivo to chemosensitize Trail-induced apoptosis in liver carcinoma cells [36]. Interestingly, 5,7-DMF could penetrate blood-brain barrier (BBB) and blood-testicular barrier, which was demonstrated by our study in mouse brains and also Mekjaruskul's study in rat brains and testicles [44]. This may imply promising medical use of 5,7-DMF for brain and testicular cancer and Alzheimer's diseases [32].

Summary

In summary, this study described the PK of 5,7-DMF in mice following 10 mg/kg oral dose for the first time. It established the tissue distribution profile and PK parameters in vivo and provided further basis for physiologically based PK modeling,

drug-drug interaction studies, dosing regimen and prediction in clinical trials in the future.

CHAPTER 4
PHARMACOKINETIC MODELING AND SIMULATION ON 5,7-DMF

Background

Pharmacokinetic models are relatively simple mathematical schemes that represent complex physiologic spaces or processes. Accurate PK modeling is important for precise determination of elimination rate. In recent years, progress has been made in PK modeling to better understand the absorption, distribution, metabolism, and excretion (ADME) of medications in vivo [57]. However, the PK model or parameters to describe the ADME of 5,7-DMF in vivo is missing to date, which hinders the further exploration or development of this promising compound. Therefore, in our study we explored the appropriateness of using population PK as a tool to explain and predict 5,7-DMF in vivo.

Empirical PK models normally take the form of one, two, or three compartment, depending on the drug disposition pattern in blood or plasma [58]. And the most commonly used are one and two compartment model. The construction of compartmental model takes into account of the drug properties such as lipophilicity, permeability and solubility. One compartment model assumes that the whole body is like a well-stirred container with drug rapidly reaching equilibrium inside it; whereas two compartment model assumes that the central compartment is like well-perfused layer that exchange drug with tissue layer with permeability-rate limited manner.

Extrapolation of pharmacokinetics from animal model to human model usually depends on either allometric scaling or physiologically based pharmacokinetic modelling (PBPK) [57]. Allometric scaling is a rather empirical approach, in which volume of distribution will be scaled up in linear fashion while clearance will be scaled up in

empirical power of 0.75. PBPK is advantageous in semi-mechanistic based to integrate compound-dependent properties and physiology-dependent characteristics. But their development tends to be resource-demanding and time-consuming. Thus in this chapter, we focused mainly on the population pharmacokinetic modeling tools to explain the ADME of 5,7-DMF in mice and then to predict the plasma concentration of 5,7-DMF in human of 70 kg body weight.

Methods

Assumptions and Model Building

In our study, we mainly focused on classical compartmental model on oral plasma PK data and the models are shown in Fig. 4-1. One-, two- and three-compartmental models will be explored and compared with and without Tlag, with zero- or first-order absorption.

A one-compartmental model assumes linear pharmacokinetics and immediate distribution and equilibrium of the drug throughout the body.

A two-compartment model consists of two parts: The first (central) compartment X1 is identified with the blood and organs that are well-perfused with the rate-limiting step of blood perfusion. The second (peripheral) compartment X2 described for tissues that are less perfused with the rate-limiting step of permeability.

A three-compartmental model takes into account the drug distribution into deep tissue and relatively shallower tissue.

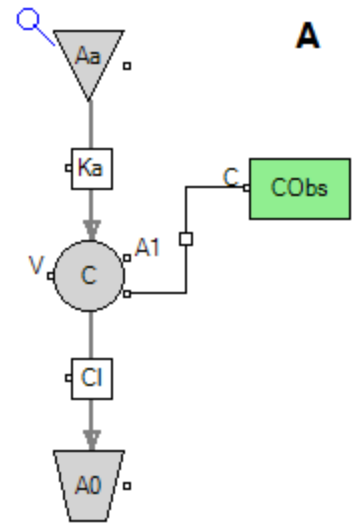

1 cmpt model

$$\frac{dA_0}{dt} = -k_a \times A_0$$

$$\frac{dA_1}{dt} = k_a \times A_0 - k_1 \times A_1$$

$$C_{obs} = \frac{A_1}{V}$$

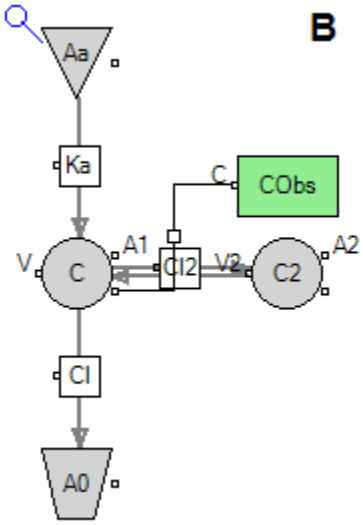

2 cmpt model

$$\frac{dA_0}{dt} = -k_a \times A_0$$

$$\frac{dA_1}{dt} = k_a \times A_0 - (k_1 + k_{12}) \times A_1$$

$$\frac{dA_2}{dt} = k_{12} \times A_1 - k_{21} \times A_2$$

$$C_{obs} = \frac{A_1}{V}$$

Figure 4-1. Structural of one-, two- and three-compartmental model and corresponding differential equations.

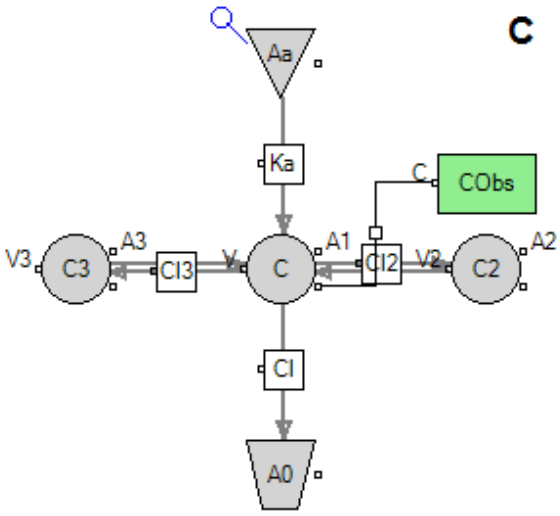

3 cmpt model

$$\frac{dA_0}{dt} = -k_a \times A_0$$

$$\frac{dA_1}{dt} = k_a \times A_0 - (k_1 + k_{12} + k_{13}) \times A_1$$

$$\frac{dA_2}{dt} = k_{12} \times A_1 - k_{21} \times A_2$$

$$\frac{dA_3}{dt} = k_{13} \times A_1 - k_{31} \times A_3$$

$$C_{obs} = \frac{A_1}{V}$$

Figure 4-1. Continued.

The structural models of one-, two- and three-compartment were compared based on fitting plots, diagnostic plots and statistical criterion such as -2LL value, Akaike Information Criterion (AIC) and Bayesian Information Criterion (BIC). On top of the base model with first-order absorption K_a, zero-order absorption was also considered into the model to compare with the fitting, precision of fitted parameters and AIC or BIC to make the final decision. As for oral absorption, the lag time (Tlag) in absorption phase was also taken into consideration. Models with or without Tlag were compared as well.

Population Modeling Analysis

The population PK (PopPK) approach was used in this study to cover the random variation into the PK model. Phoenix version 1.3 was used for this purpose. Since it was constructed on mouse plasma data with triplicate (N=3) mice sacrificed at each of ten time points, the total of 30 data points were serving as individuals pooled together.

Therefore, the naïve pool population method was chosen in terms of modeling. In this case, there was no differentiation on between-subject variability or intra-subject variability, because all sort of variability is lumped into residual/error model. In this study, we explored the residual model in additive, log-additive and multiplicative manner. Their equations are listed below.

Additive model

$$C_{Obs} = C + C_{Eps}$$

Log-additive model

$$C_{Obs} = C \times \exp(C_{Eps})$$

Multiplicative model

$$C_{Obs} = C \times (1 + C_{Eps})$$

Comparisons among different residual models were based on goodness-of-fit, diagnostic plots and statistical criterion such as -2LL value, AIC and BIC. Covariates, however, were not investigated in our study, because the plasma data were collected from mice instead of humans. So less confounding factors have been reported or collected on 5,7-DMF in mice before.

Model Validation

After the final model was selected, it was internally validated by population predictive check (VPC). Basically, it is a comparison between observed data and simulated data. VPC compared a different kind of prediction other than diagnostic plots. They are based on simulations of model predictions including random effects. Summary measures of the distribution of predictions and observations were compared visually. The results included 5% (lower), 50% (mean) and 95% (upper) percentiles.

Allometric Scalling

Scaling of a dose is expected when predicting first-in-human doses for clinical trials, dose extrapolation in veterinary practice and dose extrapolation for experimental purposes [59]. Allometric scalling was conducted on V_1, V_2, CL and CL_2. The average body weight of the experimental mice was 26.2 g, which was equivalent to 0.0262 kg. The V_1 and V_2 in mice model were scaled up to 70 kg body weight human in linear fashion; so that the power b for V_1 and V_2 was fixed at 1. The Cl and Cl2 were scaled up to 70 kg body weight human in less-than-proportion fashion; which means the power b for CL and CL_2 was fixed at 0.75 empirical value [60]. Absorption rate K_a and bioavailability F of 5,7-DMF were fixed to the values in mice.

$$Y = a \times BW^{b}$$

Model Simulation and Prediction

With the final model of two-compartmental first-order absorption without Tlag model in log-additive residual model, and the scaled up PK parameters were plugged in simulation mode of Phoenix, the model was extrapolated to predict human of 70 kg in body weight.

Results

Population Modeling Analysis

The comparisons among different models were listed in Table 4-1. Based on the results shown in Table 4-1, one-compartmental model was not good in terms of fitting and AIC/BIC. The standard error and the precision (CV%) of fitted PK parameters were huge (>100%) for one-compartmental model. Two-compartmental and three compartmental base models (without Tlag) both led to good fitting. So statistical criterion such as -2LL, AIC and BIC values played a role in decision making. Generally, AIC and BIC is balancing between goodness-of-fit and overparameterization. So the preferred model is the one with the minimum AIC/BIC value since it rewards goodness of fit (as assessed by the likelihood function), and includes a penalty for increasing number of estimated parameters.

AIC takes the function of $AIC = 2k - 2\ln(L)$, where k is the total number of parameters in the model and L is the maximal likelihood.

BIC takes the function of $BIC = -2\ln(L) + k\ln(n)$, where L is maximal likelihood, n is the number of observed data and k is the number of parameters.

Table 4-1. Model comparison under PopPK approach in Phoenix.

Model	Description	Fitting	AIC/BIC
1	1 cmpt + additive error model	Not good	393/398
2	1 cmpt + log-additive error model	Not good	108/113
3	2 cmpt + additive error model	Not good	377/390
4	2 cmpt + log-additive error model	Good	44.2/51.8
5	2 cmpt + multiplicative error model	Okay	200/207
6	2 cmpt + log-additive error model + Tlag	Good	46.0/54.8
7	3 cmpt + log-additive error model	Good	47.4/57.5
8	3 cmpt + multiplicative error model	Okay	201/211
9	3 cmpt + log-additive error model + Tlag	Good	49.2/60.5

Additive error model didn't describe data well, with some of the fitted parameters in negative value, which doesn't make sense. Compared with multiplicative error model, log-additive model provides smaller AIC/BIC with better fitting in two- and three-compartmental model. So in this case, we focused on log-additive error model.

Compared with three compartment model, two-compartmental model had similar residual, QQ (data quantile-theoretical quantile) and DV (dependent variable) vs PRED (prediction) plots. Further, two-compartmental model has smaller value in AIC/BIC than three compartment model. So the two models had AIC values of 44.2 versus 47.4, respectively. In this case, two-compartmental model was chosen as the base model.

When further compare two-compartmental model and that with Tlag, the fitting generally look similar; but AIC and BIC punish the increase in total number of parameters. So the two models had AIC values of 44.2 versus 46.0, respectively. Based on minimizing AIC/BIC principle, we chose two-compartmental model without Tlag.

Since in absorption modeling, zero-order absorption rate constant could be considered instead of first-order rate constant, we compared two-compartmental model with either zero-order (K_0) or first-order (K_a) absorption. It is interesting that the AIC/BIC values for these two models are the same; although there was a drastic increase when K_0 replace K_a in three-compartmental model, changing from 47.4/57.5 to 176/186. When looking at the fitting figure and parameter estimation table closely, we found that the fitting is better for two-compartmental model with first-order absorption; furthermore, the fitted parameters in two-compartmental model with first-order absorption had smaller standard error and CV% than two-compartmental model with the zero-order absorption

rate, thus we chose two-compartmental model with first-order absorption as our final model for further simulation and prediction.

The fitting plots for the final model are shown in Fig. 4-2. Fig. 4-2A showed goodness-of-fit plot in log transformation in DV and PRED versus time after dose. Fig. 4-2B showed goodness-of-fit plot without log transformation in DV and PRED versus time after dose. In either plot, the model fit the observed data in a decent way with reasonable variation. And the fitted parameters were listed in Table 4-2.

Table 4-2. PopPK parameters for the final model in mouse.

Parameter	Population mean estimate	SE	CV%
K_a(/h)	6.04	1.07	17.8
V_1 (L)	0.05	0.03	56.1
V_2 (L)	0.56	0.41	73.8
CL (L/h)	0.55	0.08	14.3
CL_2 (L/h)	0.04	0.02	40.2

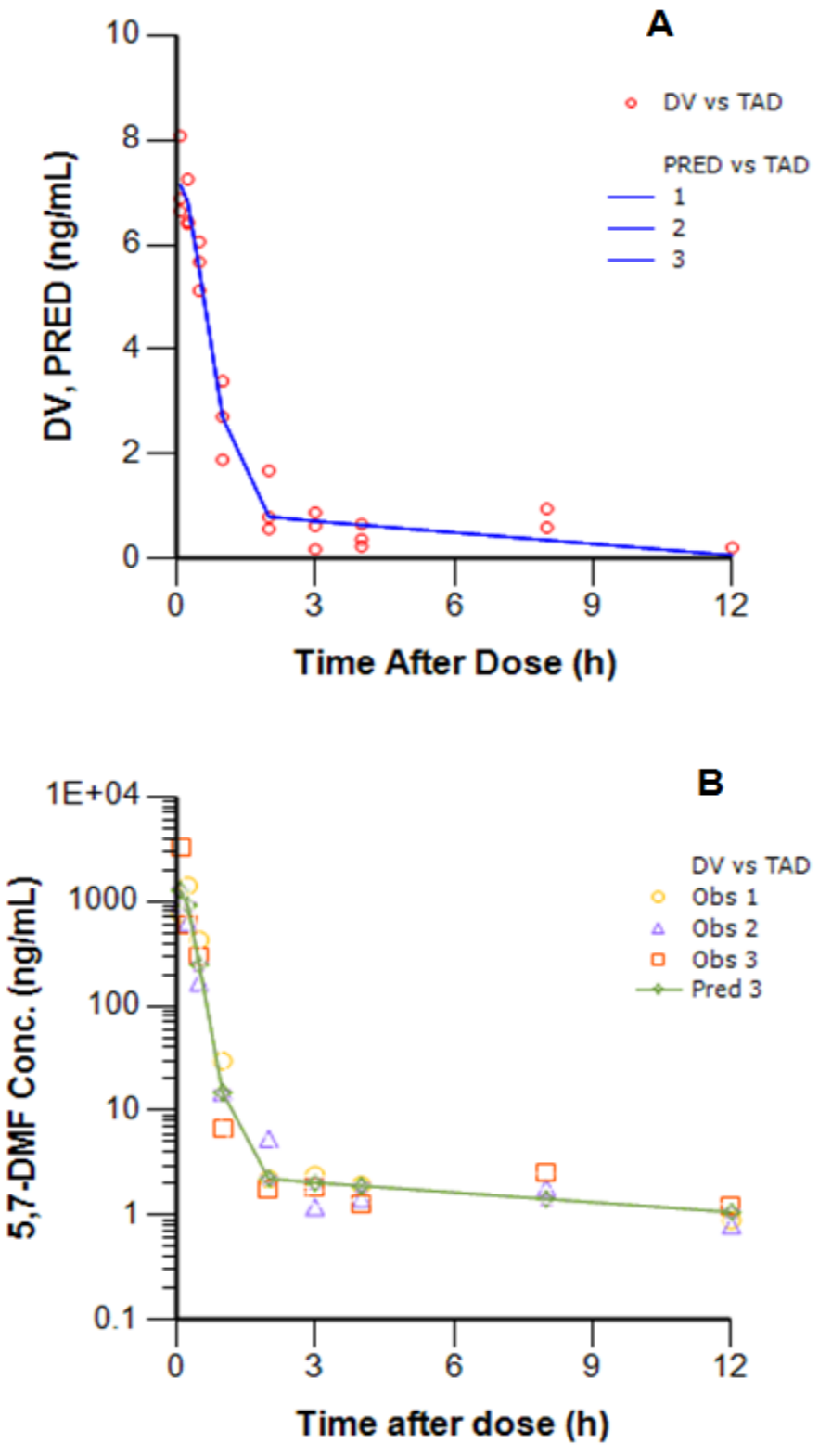

Figure 4-2. Overall goodness-of-fit plots with log transformation (A) and without log transformation (B).

And the individual fitting plot was shown in Fig 4-3 with A, B, and C panels representing the goodness-of-fit plots of ID 1, 2 and 3.

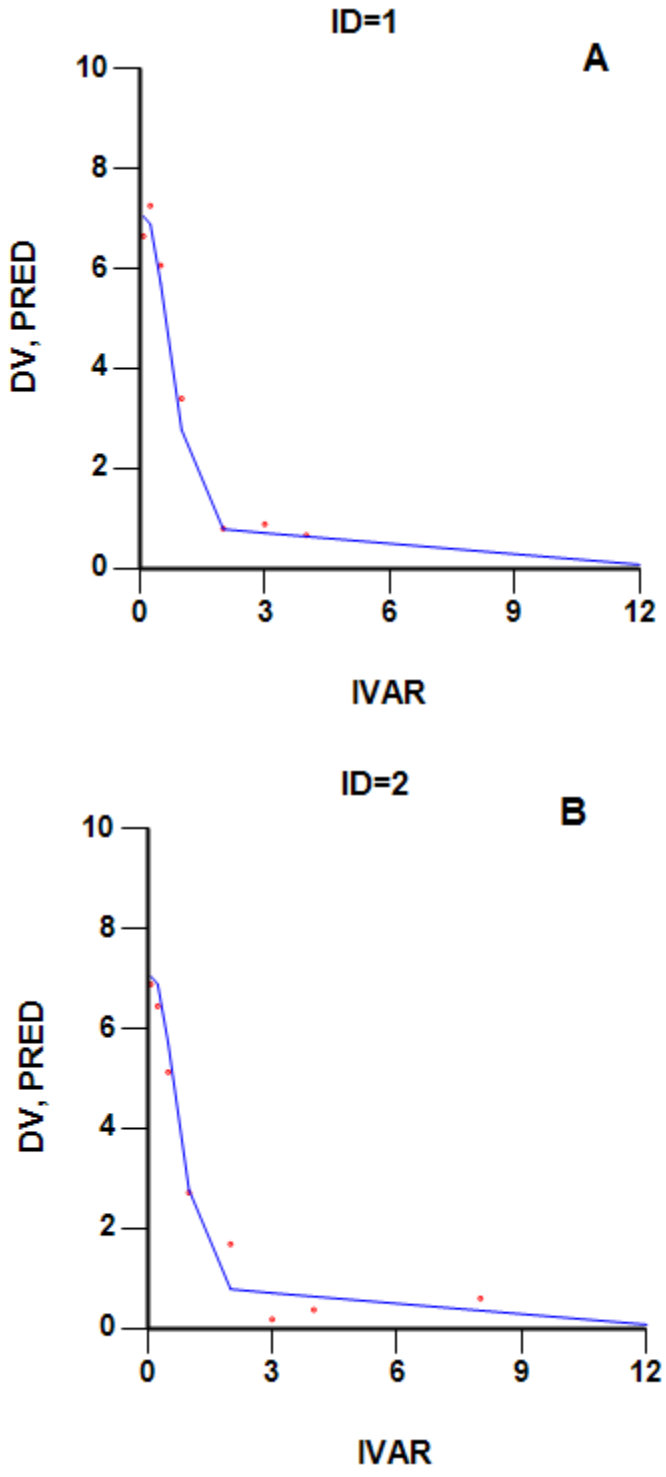

Figure 4-3. Individual goodness-of-fit plot.

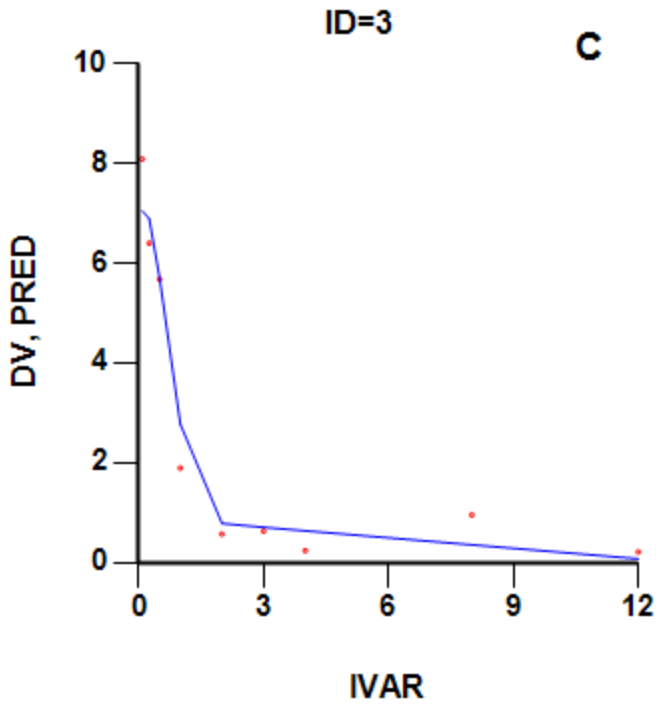

Figure 4-3. Continued.

Diagnostic plots in our study included the DV vs PRED, DV vs IPRED, CWRES (conditional weighted residual) vs PRED, CWRES vs TAD (time after dose) and QQ plots. These results were shown in Fig. 4-4. Fig. 4-4A indicated that the predicted concentration were in line with the observed concentration, which means good fit; same for Fig. 4-4B, dependent variable versus individual prediction. In the CWRES vs PRED plot, there is no trend between residual and prediction, which means the assumptions for modeling were valid; and there was no bias in this model. The random pattern was also observed in Fig. 4-4D, CWRES vs time after dose, which means there was no trend going with time. So there was no time trend to lead to any bias in the model. In both Fig. 4-4C and Fig. 4-4D plots, most of the dots were within -2 to 2 line so that only a few outliers fell out of this interval, which was a good sign indicating the goodness-of-fit. Fig. 4-4E, QQ plot showed a dissection line of y=x linear relationship, which means

the weighted residual met the expectation of standard normal quantile. There was no obvious deviation or screwness, in which normality assumption was met.

The major goal for diagnostic plots was to check the assumptions of independence, equal variance and normal distribution for the model. Residual plot can check independence and equal variance as well. By plotting residual against time or prediction, the random scattering indicated the independence of time or prediction and the assumption of equal variance were met. The robustness was demonstrated when no departure from the model assumptions were observed.

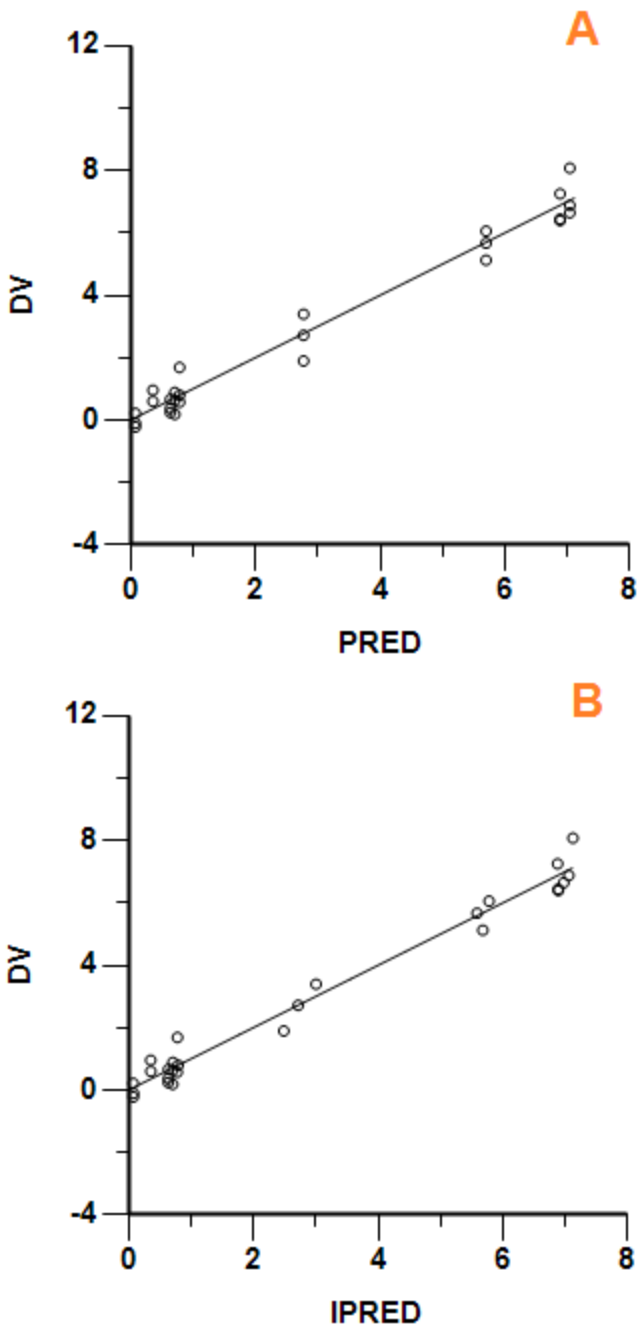

Figure 4-4. Diagnostic plots for the final model.

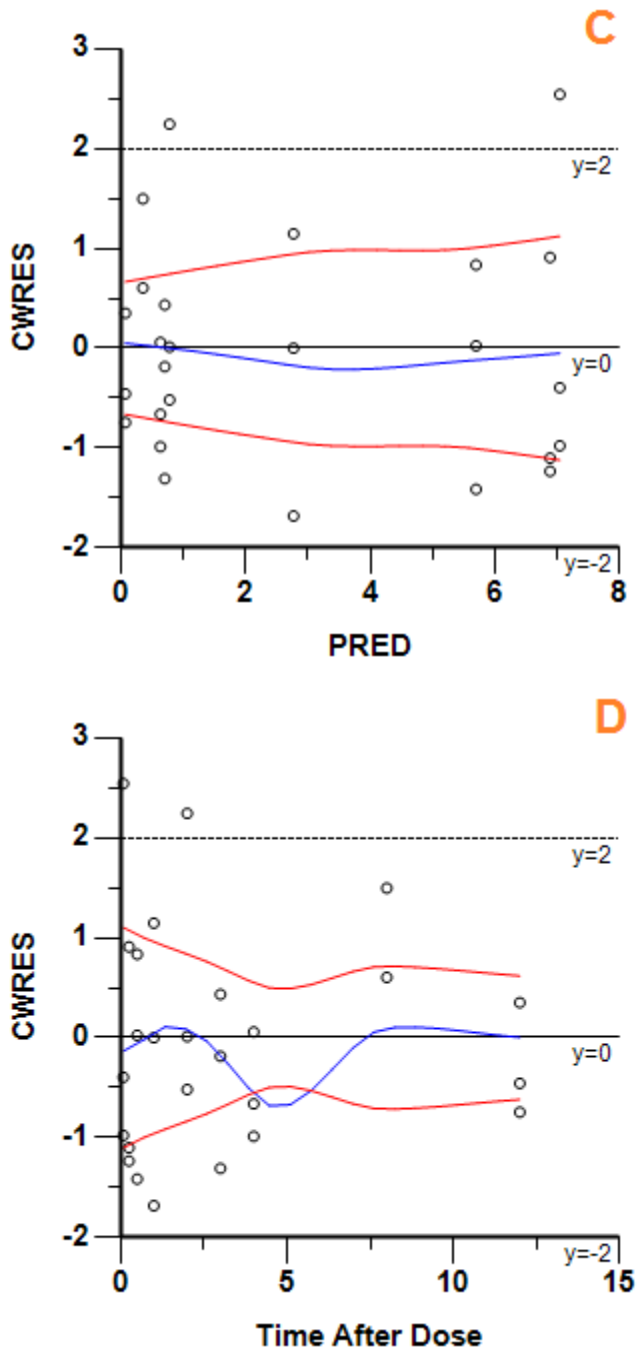

Figure 4-4. Continued.

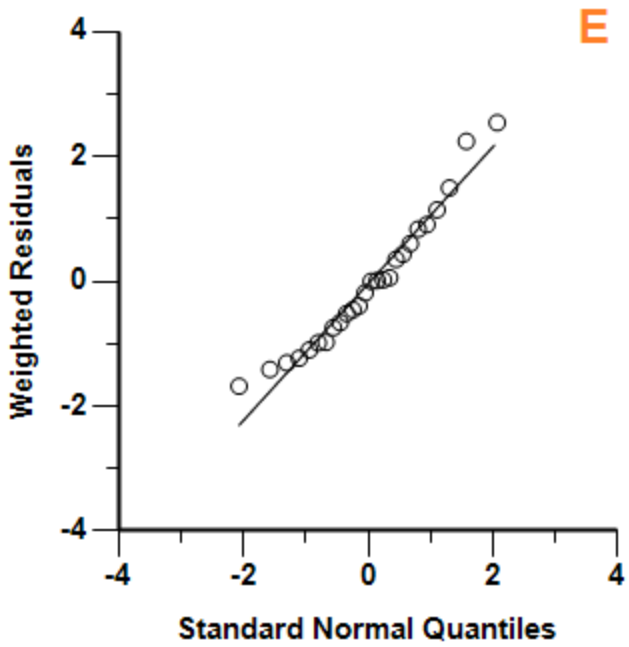

Figure 4-4. Continued.

Model Validation

Model validation was performed by VPC, as shown in Fig. 4-5. It showed that VPC had good agreement with observations. And observation intervals were within prediction intervals; there was no sign of model mis-specification, under-prediction or over-prediction.

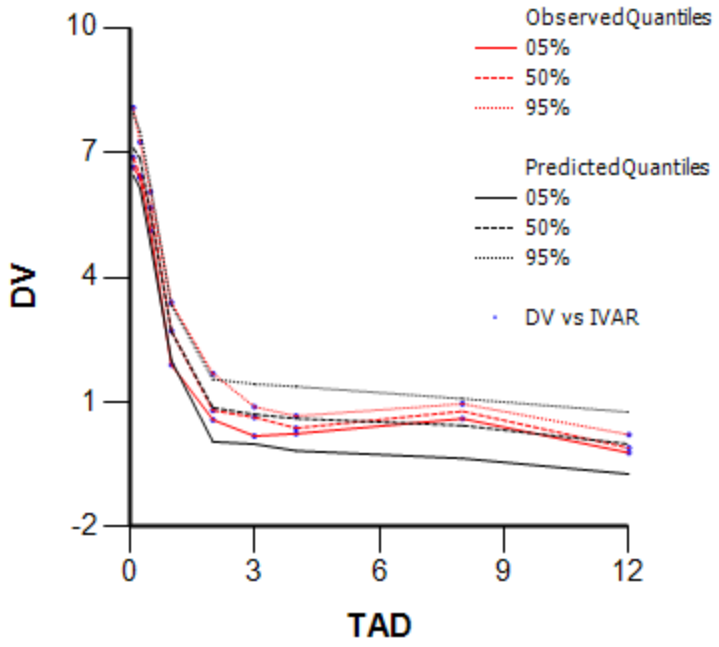

Figure 4-5. Visual predictive check for two-compartmental final PopPK model.

With this final model and its PK parameters, the simulated mouse plasma PK profile for oral administration of 10, 25 and 50 mg/kg were shown in Fig. 4-6 to 4-8. In these plots, only mean concentrations were shown.

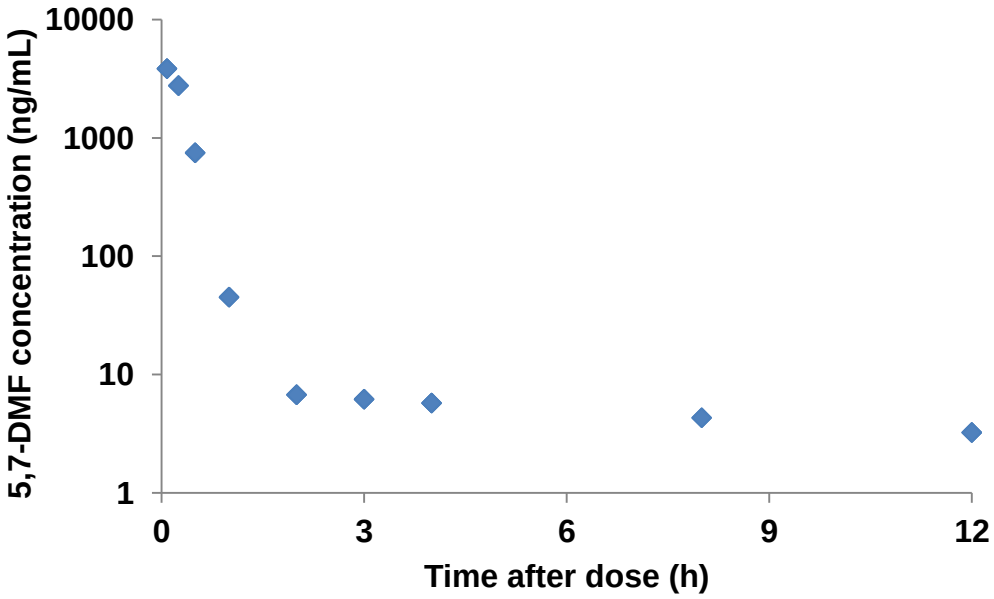

Figure 4-6. Simulated mouse plasma PK profile following oral dose of 10 mg/kg 5,7-DMF.

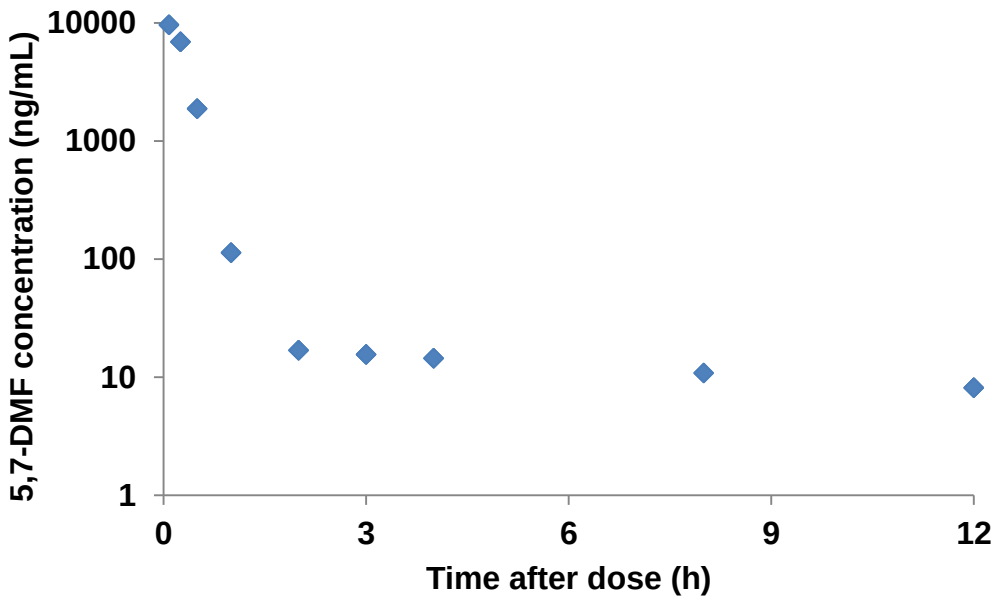

Figure 4-7. Simulated mouse plasma PK profile following oral dose of 25 mg/kg 5,7-DMF.

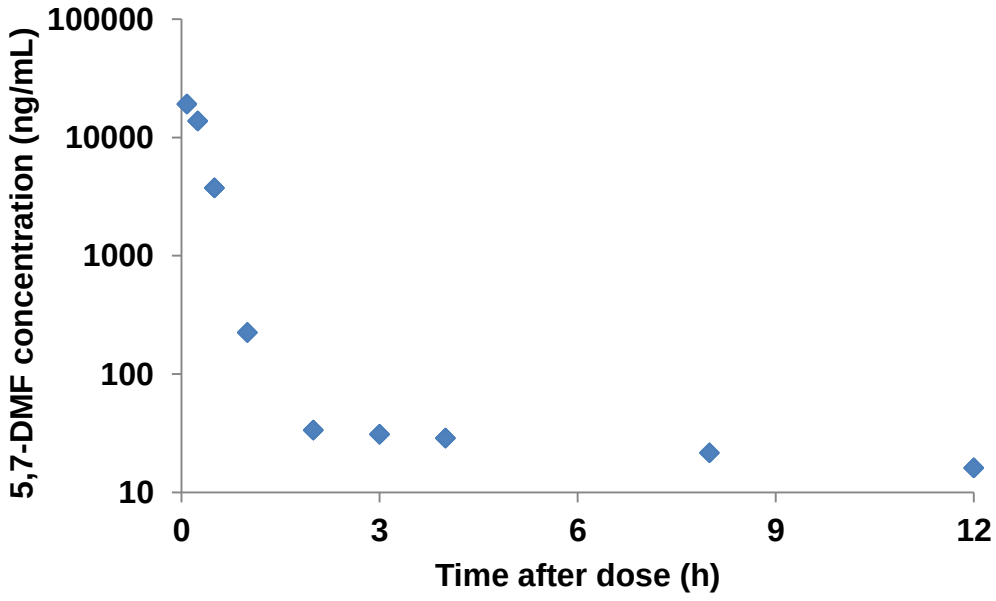

Figure 4-8. Simulated mouse plasma PK profile following oral dose of 25 mg/kg 5,7-DMF.

Allometric Scalling

Allometric scalling to human of average body weight of 70 kg resulted in parameters was shown in table 4-3. So the mean Ka was 6.04 h^{-1}, central volume of distribution was 0.05 L, peripheral volume of distribution was 0.55 L, clearance was 0.55 L/h and the intercompartmental clearance was 0.04 L/h.

Table 4-3. Scaled up PK parameters in two-compartment model for human species.

Parameter	Mean (SE) in mice	Scaled for humans
K_a(/h)	6.04 (1.07)	6.04
V_1 (L)	0.05 (0.03)	131
V_2 (L)	0.56 (0.41)	1484
CL (L/h)	0.55 (0.08)	204
CL_2 (L/h)	0.04 (0.02)	16.1

Model Simulation and Prediction

With the final model of scaled up parameters, the simulation of human plasma concentration-time profile following oral dose of 10 mg/kg 5,7-DMF solution were shown in Fig. 4-9. Panel A showed the simulation figure generated by the software under log scale whereas panel B was the figure after transformation back to linear scale. Both graphs indicated the 5, 50 and 95 percentiles. Predicted human plasma concentration following oral dose of 10 mg/kg 5,7-DMF. The predicted half-life is 3.45 h, T_{max} is 0.25 h, C_{max} is 9860 ng/mL, AUC_{inf} is 21200 h*ng/mL.

Currently, however, there has not been any clinical data to externally validate this model. But our simulation could serve in the near future as the starting point for prediction of human plasma concentration for future clinical trials possibly. Besides, our report will be the first to describe the modeling and simulation on 5,7-DMF, which may shed light on further model refinement.

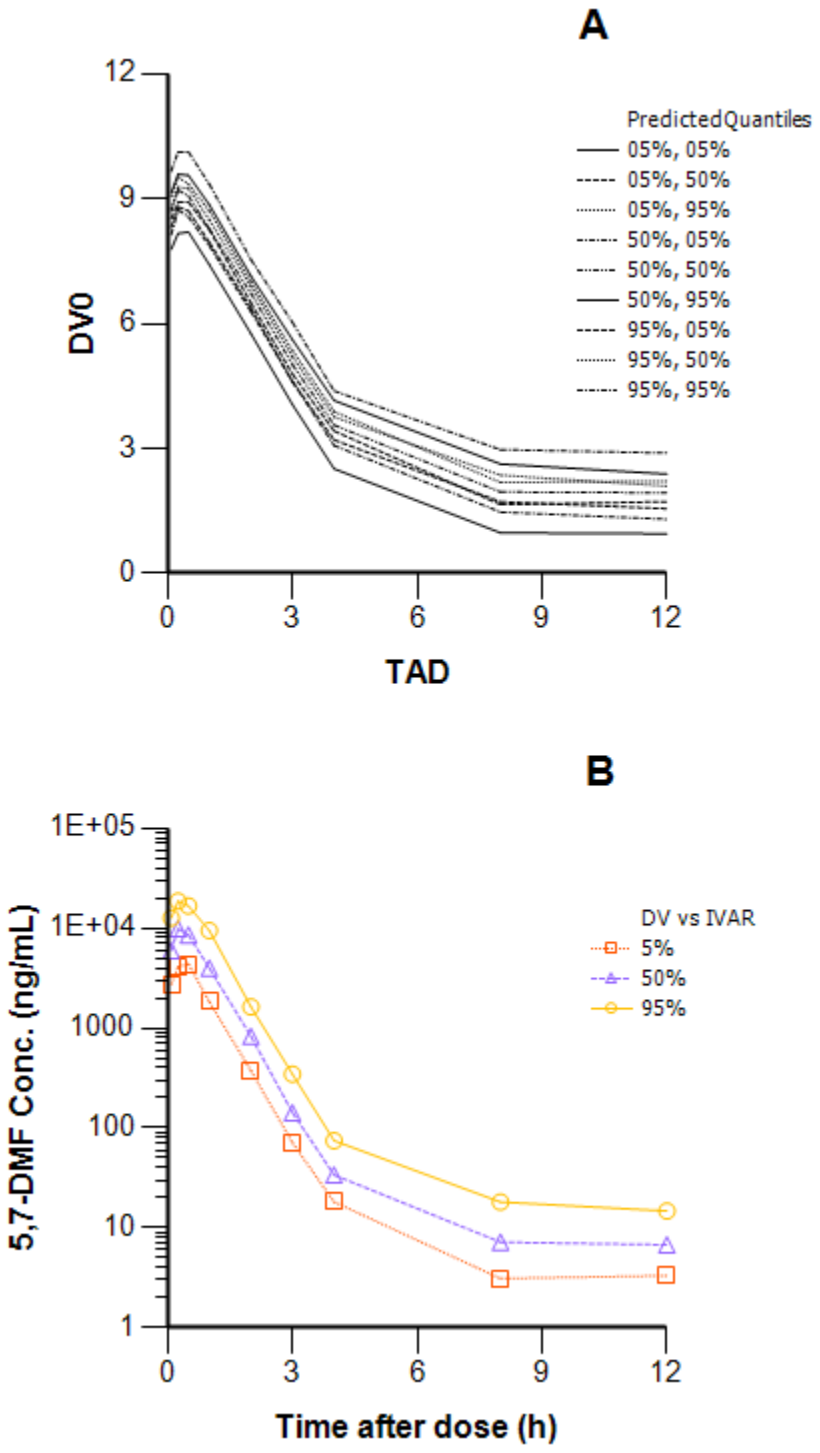

Figure 4-9. Simulation of 5,-7DMF concentration-time profile in 70 kg human being after oral dose of 10 mg/kg 5,7-DMF (N=3).

Discussions

In the model selection part, first-order absorption rate was more reasonable than zero-order absorption rate because usually, the controlled release or IV infusion enhibit constant doing rate into the body.

Allometric scaling across different species can help understand the implication from preclinical data to clinical trials and it is rational tool despite its limitations [61-62]. Usually the extrapolation among species is based on parameter estimation on data of at least three species [63]. The single point extrapolation based on one animal species to corresponding human being could not ensure accuracy [64].

Besides this single-point method, there are other extrapolation methods on clearance using brain weight, longevity, GFR, bile flow or UDPGT [61]. Depending on different properties of the drug, the predictability of each method varies. For this study, there is too limited animal species available. Furthermore, the physic-chemical characteristics of 5,7-DMF have not been fully captured yet. Based on the PK profile, the parent compound seems to undergo fast clearance. With historic knowledge that the excretion of 5,7-DMF through urine and feces was less than 5% of the total dosing, we assume that the majority of the parent compound went through metabolic pathway, so that this simple allometry method should be a good estimate.

First-order absorption rate constant Ka was not scaled up to predict human concentration. It was not well discussed by literature probably because of the large difference in absorption among species [59, 65, 66].

Summary

PK model was formulated for the first time to describe 5,7-DMF in vivo.

Two compartmental model best fit the observed plasma data. Its validity was evaluated through diagnostic plots, fitting figures and statistical criteria. The final model incorporated first-order absorption without lag time.

This model was helpful to describe current observation in mice and may predict the plasma levels of 5,7-DMF in human. For example, the fitted parameters could also be useful for future PBPK modeling. K_a can be used as initial estimate in coding. The predicted volume of distribution can be also estimate as tissues for perfusion-rate limited model.

CHAPTER 5
CONCLUSIONS

Summary

We established for the first time a sensitive, fast and selective quantification method using LC-MS/MS to quantify 5,7-DMF in mouse plasma and tissues. Further we reported for the first time the dose linearity, PK and tissue distribution of 5,7-DMF in mice. Last but not the least, we constructed for the first time PK modeling and simulation of 5,7-DMF in vivo.

Our bioanalytical method was fully validated and all of the fundamental parameters in method validation, including accuracy, precision, sensitivity, selectivity, recovery and stability were evaluated thoroughly in mouse plasma. The calibration curve covered 2–1000 ng/mL with the lower limit of quantification (LLOQ) of 2 ng/mL. The inter-run and intra-run precision and accuracy were less than 15% of nominal concentrations. The matrix effect and recovery yield were within ±15% of nominal concentrations. This sensitive and specific quantification method was also adapted to quantify mouse tissues for further PK studies in vivo.

To investigate the PK properties and tissue distribution, 5,7-DMF was first dosed intravenously (IV) in a parallel study of 10 to 50 mg/kg 5,7-DMF to mice. The AUC was demonstrated dose proportional within the dose range. And then in the following study of 10 mg/kg oral dosing, mouse plasma, heart, lung, liver, kidney, intestine, brain, spleen, muscle and fat tissues were collected and analyzed using LC-MS/MS. The calculated bioavailability was 13.8%. Following oral dosing, the maximal 5,7-DMF concentrations in plasma and tissues were reached within 30 min. The peak plasma

concentration (C_{max}) was 1870 ± 1190 ng/mL, and area under the curve (AUC_t) was 532 ± 165 hr*ng/mL and terminal half-life was 3.40 ± 2.80 hr. The volume of distribution was 90.1 ± 62.0 L/kg. Clearance was 20.2 ± 7.49 L/hr/kg. Except for muscle and adipose, other tissues had higher C_{max} than plasma, ranging from 1.75- to 9.96-fold. After oral administration, 5,7-DMF was most abundant in gut, followed by liver, kidney, brain, spleen, heart, lung, adipose and muscle. The partition coefficient (K_p) of these tissues were 0.65 to 12.9.

We further constructed compartmental modeling on mouse plasma and two-compartmental model with first order absorption and without Tlag model best described the oral plasma data. The fitted PK parameter K_a was 6.04 1/h, V_1 was 0.05 L, V_2 was 0.56 L, CL was 0.55 L/h, and CL_2 was 0.04 L/h. This final model was extrapolated to human of average body weight of 70 kg with V_1, V_2, CL and CL_2 scaled up, which may provide insight for 5,7-DMF concentration prediction in human plasma.

PK model was formulated for the first time to describe 5,7-DMF in vivo. Two compartmental model best fit the observed plasma data. Its validity was evaluated through diagnostic plots, fitting figures and statistical criteria. The final model incorporated first-order absorption without lag time. This model was helpful to describe current observation in mice and may predict the plasma levels of 5,7-DMF in human. The fitted parameters could also be useful for future PBPK modeling.

Perspective

Given the challenges in the complex scenario, PBPK tools are popular for orally administered compounds as the absorption depends on drug-related factors and also physiology of GI tract [67]. It is generally accepted as ‘bottom-up’ approach and incorporated measured parameters that can impact drug ADME [68]. The major

advancement and wide application nowadays are due to refined characterization of human body [69-70], progressive understanding of total body water [71] and development of a variety of *in silico* software [67] including Simcyp, Gastroplus, Matlab and so on. Other software such as ADAPT is less user-friendly compared with Simcyp and Gastroplus. But either way, the essence for PBPK modeling utilizes differential equations and in vitro-measured and preclinical data to gain mechanistic insight. It is especially useful to extrapolate across dosing routes and across different animal species and to understand dose selection in clinical trials [72], special populations such as pediatric patients and pregnant women [73-75] and to investigate DDI studies [76]. Its application does not only exist in drug discovery and development, but also helps risk assessment and environmental protection [77-79].

With the fitted empirical model, our ultimate goal is to construct a PBPK model using mouse plasma and tissue PK data, and then extrapolate to human species to predict human plasma and tissue levels of 5,7-DMF. The physiologically-based pharmacokinetic (PBPK) model was introduced in 1924 [80] which incorporated physiologically meaningful organs into a mass balance differential equation connected by body fluid fluxes to describe fate of the substance (Fig. 5-1) and local model could be perfusion rate-limited or permeability rate-limited, as shown in Fig 5-2. It generally has three different types: whole-body PBPK, partial PBPK and metabolic PBPK [81-83]. The mathematical description of mass balance for each compartment also depends on the mechanisms of drug ADME. But compared to conventional approach, PBPK has advantages in that, first of all, it is an useful tool to extrapolate model across species; secondly, it allow the extrapolation among different doses and dosing routes; thirdly,

since each compartment in the model has physiological meaning, the model enables us to predict the tissue concentration in human without actually collect human tissues; lastly, it is widely applied nowadays since it includes both extrinsic and intrinsic factors [84].

The PBPK model consists of drug-specific parameters and system-specific ones. Typical drug-specific parameters can be estimated by either in vitro and in vivo experiments [85-86] or quantitative relationships [87] or allometric scaling [88]. The physiological parameters usually consist of blood flow and volumes of blood/plasma and different tissues with measured values reported by previous literature [89-90].

The PBPK models have been developed for many anticancer drugs such as mitoxantrone [60], and cisplatin [91]. However, PBPK model for 5,7-DMF has not been reported before. In our study, we have measured 5,7-DMF concentrations in mouse plasma and nine tissues, which provided valuable information to build whole-body PBPK model in the near future. Once this PBPK model is successfully developed and validated, it can be then extrapolated to predict the corresponding plasma and tissue concentrations in human species. It will be clinically relevant to use that model for dosing regimen and other adjustment as well.

The research on 5,7-DMF as model compound of methylated flavonoids could shed light on future investigation on analogue with similar stability to liver metabolism yet demonstrating promising anti-proliferative, and chemopreventive traits. The bioanalytical condition can be applied to establish the quantification methods; and the PK methodology can be helpful to study similar compounds in vivo; the modeling

approaches in the empirical and PBPK construction may provide insight for other scientists researching on phytochemicals or natural flavonoids.

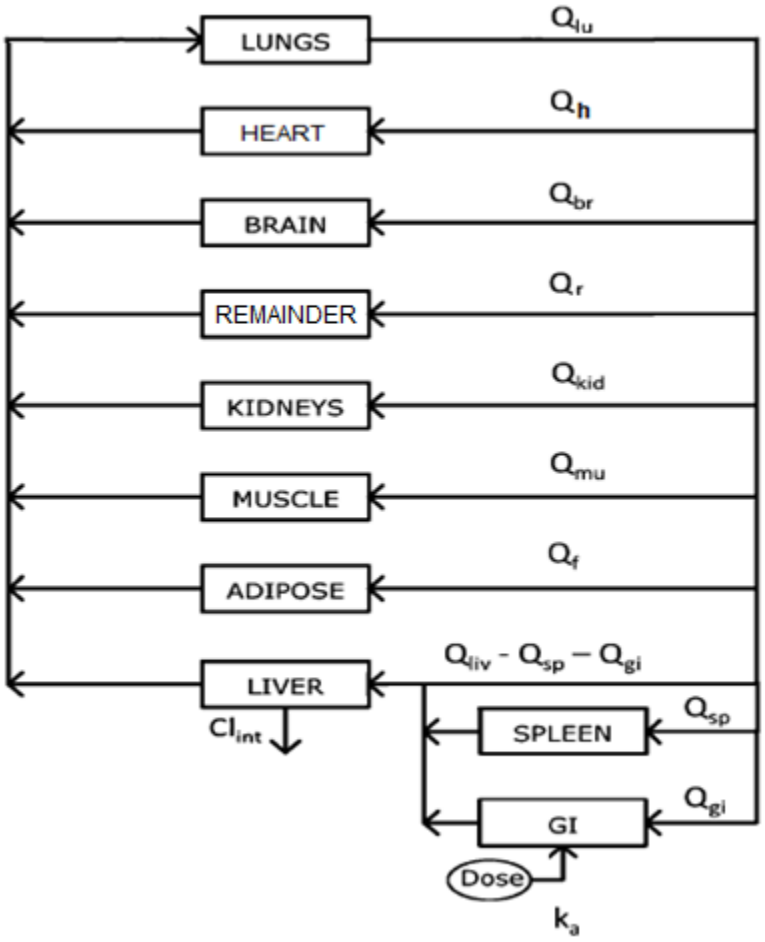

Figure 5-1. Exemplary whole-body PBPK model for oral dosing.

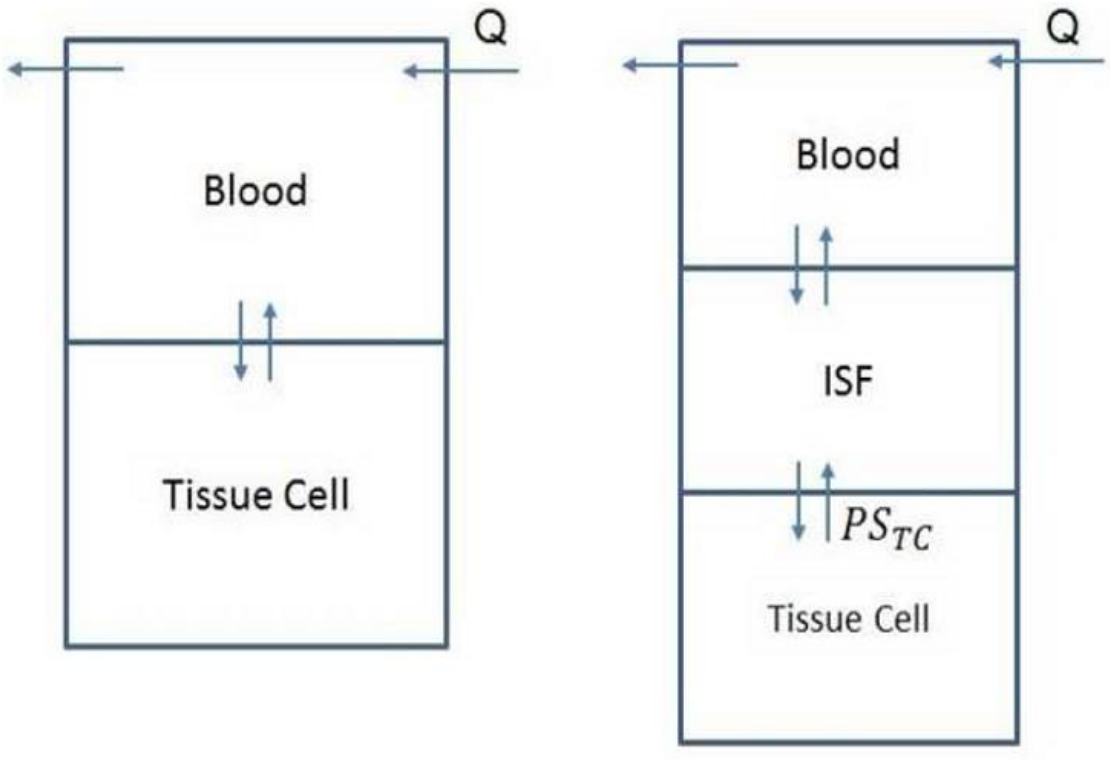

Figure 5-2. Exemplary local PBPK model for oral dosing.

LIST OF REFERENCES

[1] Y.Y. Zhao, Traditional uses, phytochemistry, pharmacology, pharmacokinetics and quality control of Polyporus umbellatus (Pers.) Fries: a review, J. Ethnopharmacol. 149 (2013) 35-48.

[2] X. Wang, H. Zhang, L. Chen, L. Shan, G. Fan, X. Gao, Liquorice, a unique "guide drug" of traditional Chinese medicine: a review of its role in drug interactions, J. Ethnopharmacol. 150 (2013) 781-90.

[3] B.J. Gurley, Pharmacokinetic herb-drug interactions (part 1): origins, mechanisms, and the impact of botanical dietary supplements, Planta. Med. 78 (2012) 1478-89.

[4] B.J. Gurley, E.K. Fifer, Z. Gardner, Pharmacokinetic herb-drug interactions (part 2): drug interactions involving popular botanical dietary supplements and their clinical relevance, Planta. Med. 78 (2012) 1490-514.

[5] A. Nahrstedt, V. Butterweck, Lessons learned from herbal medicinal products: the example of St. John's Wort (perpendicular), J. Nat. Prod. 73 (2010) 1015-21.

[6] E.J. Park, J.M. Pezzuto, Flavonoids in cancer prevention, Anticancer. Agents. Med. Chem. 12 (2012) 836-51.

[7] L.H. Yao, Y.M. Jiang, J. Shi, F.A. Toma´s-Barbera´n, N. Datta, R. Singanusong, S.S. Chen. Flavonoids in food and their health benefits, Plant. Foods. Hum. Nutr. 59 (2004) 113–22.

[8] Y.J. Surh. Cancer chemoprevention with dietary phytochemicals, Nat. Rev. Cancer. (2003) 768–80.

[9] C. Heiss, C.L. Keen, M. Kelm, Flavanols and cardiovascular disease prevention, Eur. Heart. J. (2010) 2583–92.

[10] P.M. Kris-Etherton, M. Lefevre, G.R. Beecher, M.D. Gross, C.L. Keen, T.D. Etherton, Bioactive compounds in nutrition and health-research methodologies for establishing biological function: the antioxidant and anti-inflammatory effects of flavonoids on atherosclerosis, Annu. Rev. Nutr. 24 (2004) 511–38.

[11] M. Rossi, C. Bosetti, E. Negri, P. Lagiou, C. La Vecchia, Flavonoids, proanthocyanidins, and cancer risk: a network of case-control studies from Italy, Nutr. Cancer. 62 (2010) 871–7.

[12] W. Garavello, M. Rossi, J.K. McLaughlin, C. Bosetti, E. Negri, P. Lagiou, Flavonoids and laryngeal cancer risk in Italy, Ann. Oncol. 18 (2007) 1104–9.

[13] A.M. Ekstro¨m, M. Serafini, O. Nyre´n, A. Wolk, C. Bosetti, R. Bellocco, Dietary quercetin intake and risk of gastric cancer: results from a population-based study in Sweden, Ann. Oncol. 22 (2011) 438–43.

[14] M. Rossi, A. Lugo, P. Lagiou, A. Zucchetto, J. Polesel, D. Serraino, Proanthocyanidins and other flavonoids in relation to pancreatic cancer: a case-control study in Italy, Ann. Oncol. 23 (2012) 1488-93.

[15] P. Lagiou, M. Rossi, A. Lagiou, A. Tzonou, C. La Vecchia, D. Trichopoulos, Flavonoid intake and liver cancer: a case-control study in Greece, Cancer. Causes. Control. 19 (2008) 813–8.

[16] C.L. Heald, M.R. Ritchie, C. Bolton-Smith, M.S. Morton, F.E. Alexander, Phytooestrogens and risk of prostate cancer in Scottish men, Br. J. Nutr. 98 (2007) 388–96.

[17] M.D. Jackson, N.D. McFarlane-Anderson, G.A. Simon, F.I. Bennett, S.P. Walker, Urinary phytoestrogens and risk of prostate cancer in Jamaican men, Cancer. Causes. Control. (2010) 2249–57.

[18] M. Rossi, E. Negri, P. Lagiou, R. Talamini, L. Dal Maso, M. Montella, Flavonoids and ovarian cancer risk: a case-control study in Italy, Int. J. Cancer. 123 (2008) 895–8.

[19] Y. Cui, H. Morgenstern, S. Greenland, D.P. Tashkin, J.T. Mao, L. Cai, Dietary flavonoid intake and lung cancer–a population-based case-control study, Cancer. 112 (2008) 2241–8.

[20] E.V. Bandera, M.G. Williams, C. Sima, S. Bayuga, K. Pulick, H. Wilcox, Phytoestrogen consumption and endometrial cancer risk: a population-based casecontrol study in New Jersey, Cancer. Causes. Control. 20 (2009) 1117–27.

[21] Q. Wang, H. Li, P. Tao, Y.P. Wang, P. Yuan, C.X. Yang, Soy isoflavones, CYP1A1, CYP1B1, and COMT polymorphisms, and breast cancer: a case-control study in southwestern China, DNA. Cell. Biol. 30 (2011) 585–95.

[22] Y.A. Cho, J. Kim, K.S. Park, S.Y. Lim, A. Shin, M.K. Sung, J. Ro, Effect of dietary soy intake on breast cancer risk according to menopause and hormone receptor status, Eur J. Clin. Nutr. 64 (2010) 924–32.

[23] M. Iwasaki, G.S. Hamada, I.N. Nishimoto, M.M. Netto, J.J. Motola, F.M. Laginha, Isoflavone, polymorphisms in estrogen receptor genes and breast cancer risk in case-control studies in Japanese, Japanese Brazilians and non-Japanese Brazilians, Cancer. Sci. 100 (2009) 927–33.

[24] M. Iwasaki, G.S. Hamada, I.N. Nishimoto, M.M. Netto MM, Motola, F.M. Laginha, Dietary isoflavone intake and breast cancer risk in case-control studies in Japanese, Japanese Brazilians, and non-Japanese Brazilians, Breast. Cancer. Res. Treat. 116 (2009) 401–11.

[25] B.N. Fink, S.E. Steck, M.S. Wolff, J.A. Britton, G.C. Kabat, J.C. Schroeder, Dietary flavonoid intake and breast cancer risk among women on Long Island, Am. J. Epidemiol. 165 (2007) 514–23.

[26] J.W. Lampe, Y. Nishino, R.M. Ray, C. Wu, W. Li, M.G. Lin, Plasma isoflavones and fibrocystic breast conditions and breast cancer among women in Shanghai, China, Cancer. Epidemiol. Biomarkers. Prev. 16 (2007) 2579–86.

[27] D. Patanasethanont, J. Nagai, R. Yumoto, T. Murakami, K. Sutthanut, Effects of Kaempferia parviflora extracts and their flavone constituents on P-glycoprotein function, J. Pharm. Sci. 96 (2007) 223–33.

[28] D. Wu, M.G. Nair, D.L. DeWitt, Novel compounds from Piper methysticum Forst (Kava Kava) roots and their effect on cyclooxygenase enzyme, J. Agric. Food. Chem. 50 (2002) 701–5.

[29] H. Haberlein, K.P. Tschiersch, H.L. Schafer, Flavonoids from Leptospermum scoparium with affinity to the benzodiazepine receptor characterized by structure activity relationships and in vivo studies of a plant extract, Pharmazie. 49 (1994) 912–22.

[30] C. Sae-Wong, H. Matsuda, S. Tewtrakul, P. Tansakul, S. Nakamura, Y. Nomura, M. Yoshikawa, Suppressive effects of methoxyflavonoids isolated from Kaempferia parviflora on inducible nitric oxide synthase (iNOS) expression in RAW 264.7 cells, J. Ethnopharmacol. 136 (2011) 488-95.

[31] P. Tep-Areenan, P. Sawasdee, M. Randall, Possible mechanisms of vasorelaxation for 5,7-dimethoxyflavone from Kaempferia parviflora in the rat aorta, Phytother. Res. 24 (2010) 1520-5.

[32] P. Sawasdee, C. Sabphon, D. Sitthiwongwanit, U. Kokpol, Anticholinesterase Activity of 7-Methoxyflavones Isolated from Kaempferia parviflora, Phytother. Res. 23 (2009) 1792-4.

[33] X. Wen, U.K. Walle, T. Walle, 5, 7-Dimethoxyflavone downregulates CYP1A1 expression and benzo[a]pyrene-induced DNA binding in Hep G2 cells, Carcinogenesis. 26 (2005) 803–9.

[34] X. Wen, T. Walle, Cytochrome P450 1B1, a novel chemopreventive target for benzo[a]pyrene-initiated human esophageal cancer, Cancer. Lett. 246 (2007) 109–14.

[35] X. Wen, T. Walle, Preferential induction of CYP1B1 by benzo[a]pyrene in human oral epithelial cells: impact on DNA adduct formation and prevention by polyphenols, Carcinogenesis. 26 (2005) 1774–81.

[36] J.F. Yang, J.G. Cao, L. Tian, F. Liu, 5, 7-Dimethoxyflavone sensitizes TRAIL-induced apoptosis through DR5 upregulation in hepatocellular carcinoma cells, Cancer. Chemother. Pharmacol. 69 (2012) 195-206.

[37] B. Wudtiwai, B. Sripanidkulchai, P. Kongtawelert, R. Banjerdpongchai, Methoxyflavone derivatives modulate the effect of TRAIL-induced apoptosis in human leukemic cell lines, J. Hematol. Oncol. 4 (2011) 52.

[38] D. Patanasethanont, J. Nagai, C. Matsuura, K. Fukui, K. Sutthanut, B.O. Sripanidkulchai, R. Yumoto, M. Takano, Modulation of function of multidrug resistance associated-proteins by Kaempferia parviflora extracts and their components, Eur. J. Pharmacol. 566 (2007) 67-74.

[39] G. An, F. Wu, M.E. Morris, 5,7-Dimethoxyflavone and multiple flavonoids in combination alter the ABCG2-mediated tissue distribution of mitoxantrone in mice, Pharm. Res. 28 (2011) 1090-9.

[40] G. An, M.E. Morris, Effects of single and multiple flavonoids on BCRP-mediated accumulation, cytotoxicity and transport of mitoxantrone in vitro, Pharm. Res. 27 (2010) 1296-1308.

[41] G. Szakács, J.K. Paterson, J.A. Ludwig, C. Booth-Genthe, M.M. Gottesman, Targeting multidrug resistance in cancer, Nat. Rev. Drug. Discov. 5 (2006) 219-34.

[42] P.A. Tsuji, T. Walle, Inhibition of benzo[a]pyrene-activating enzymes and DNA binding in human bronchial epithelial BEAS-2B cells by methoxylatedflavonoids, Carcinogenesis 27 (2006) 1579–1585.

[43] T. Walle, N. Ta, T. Kawamori, X. Wen, P.A. Tsuji, U.K. Walle, Cancer chemo-preventive properties of orally bioavailable flavonoids-methylated versusunmethylated flavones, Biochem. Pharmacol. 73 (2007) 1288–1296.

[44] C. Mekjaruskul, M. Jay, B. Sripanidkulchai, Pharmacokinetics, bioavail-ability, tissue distribution, excretion, and metabolite identification ofmethoxyflavones in Kaempferia parviflora extract in rats, Drug Metab. Dispos.40 (2012) 2342–2353.

[45] X. Wen, T. Walle, Methylation protects dietary flavonoids from rapid hepatic metabolism, Xenobiotica. 36 (2006):387-97.

[46] T. Walle, Absorption and metabolism of flavonoids, Free Radicals in Biology and Medicine. 36 (2004):829–837.

[47] X. Wen, T. Walle, Methylated flavonoids have greatly improved intestinal absorption and metabolic stability, Drug Metab Dispos. 34 (2006):1786-92.

[48] K. Sutthanut, B. Sripanidkulchai, C. Yenjai, M. Jay, Simultaneous identificationand quantitation of 11 flavonoid constituents in Kaempferia parviflora by gaschromatography, J. Chromatogr. A 1143 (2007) 227–233.

[49] S. Ponnayyan Sulochana, K. Sharma, R. Mullangi, S.K. Sukumaran, Review of the validated HPLC and LC-MS/MS methods for determination of drugs used in clinical practice for Alzheimer's disease, Biomed. Chromatogr. 28 (2014) 1431-90.

[50] K.S. Leung, B.M. Fong, LC–MS/MS in the routine clinical laboratory: has its time come, Anal. Bioanal. Chem. 406 (2014) 2289-301.

[51] M.M Kushnir, A.L. Rockwood, J. Bergquist, Mass. Spectrom. Rev. 29 (2010) 480–502.

[52] J.M.W. van den Ouweland, I.P. Kema, J. Chromatogr. B. 883 (2012) 18–32.

[53] M. Himmelsbach, J. Chromatogr. B. 883–884 (2012) 3–17.

[54] FDA Guidance for Industry Bioanalytical Method Validation, 2001,http://www.fda.gov/downloads/Drugs/GuidanceComplianceRegulatoryInformation/Guidances/ucm070107.pdf.

[55] D. Bei, G. An, Quantification of 5,7-dimethoxyflavone in mouse plasma using liquid chromatography-tandem mass spectrometry (LC-MS/MS) and its application to a pharmacokinetic study, J. Chromatogr. B. Analyt. Technol. Biomed. Life. Sci. 978-979 (2015) 11-7.

[56] FDA Draft Guidance for Industry Bioanalytical Method Validation, 2013, http://www.fda.gov/downloads/drugs/guidancecomplianceregulatoryinformation/guidances/ucm368107.pdf.

[57] C.A. Knibbe, K.P. Zuideveld, L.P. Aarts, P.F. Kuks, M. Danhof, Allometric relationships between the pharmacokinetics of propofol in rats, children and adults, Br. J. Clin. Pharmacol. 59 (2015):705-11.

[58] F. Seker, J. Hesser, M.A. Brockmann, E. Neumaier-Probst, C. Groden, R. Schubert, C. Brockmann, Pharmacokinetic Modeling of Intra-arterial Nimodipine Therapy for Subarachnoid Hemorrhage-Related Cerebral Vasospasm, Clin. Neuroradiol. (2015).

[59] V. Sharma, J.H. McNeill, To scale or not to scale: the principles of dose extrapolation, Br. J. Pharmacol. 157(2009):907-21.

[60] G. An, M.E. Morris, A physiologically based pharmacokinetic model of mitoxantrone in mice and scale-up to humans: a semi-mechanistic model incorporating DNA and protein binding, AAPS. 14 (2012):352-64.

[61] Q. Huang, J.E. Riviere, The application of allometric scaling principles to predict pharmacokinetic parameters across species, Expert. Opin. Drug. Metab. Toxicol. 10 (2014) 1241-53.

[62] H. Tang, M. Mayersohn, Controversies in allometric scaling for predicting human drug clearance: an historical problem and reflections on what works and what does not, Curr. Top. Med. Chem. 11 (2011) 340-50.

[63] B. Clancy, B.L. Finlay, R.B. Darlington, K.J. Anand, Extrapolating brain development from experimental species to humans, Neurotoxicology. 28 (2007):931-7.

[64] G.S. Duthu, Interspecies correlation of the pharmacokinetics of erythromycin, oleandomycin, and tylosin, J. Pharm. Sci. 74 (1985):943-6.

[65] B. Clark, D.A. Smith, Pharmacokinetics and toxicity testing, Crit. Rev. Toxicol. 12(1984):343–385.

[66] J.H. Lin, Applications and limitations of interspecies scaling and in vitro extrapolation in pharmacokinetics, Drug. Metab. Dispos. 26 (1998):1202–1212.

[67] E.S. Kostewicz, L. Aarons, M. Bergstrand, M.B. Bolger, A. Galetin, O. Hatley, M. Jamei, R. Lloyd, X. Pepin, A. Rostami-Hodjegan, E. Sjögren, C. Tannergren, D.B. Turner, C. Wagner, W. Weitschies, J. Dressman, PBPK models for the prediction of in vivo performance of oral dosage forms, Eur. J. Pharm. Sci. 57 (2014) 300-21.

[68] M. Rowland, C. Peck, G. Tucker, Physiologically-based pharmacokinetics in drug development and regulatory science, Annu. Rev. Pharmacol. Toxicol. 51 (2011) 45–73.

[69] T. Teorell, Kinetics of distribution of substances administered to the body. I The extravascular modes of administration, Arch. Int. Pharmacodyn. Ther. 57 (1937) 205–225.

[70] T. Teorell, Kinetics of distribution of substances administered to the body. I The intravascular modes of administration, Arch. Int. Pharmacodyn. Ther. 57 (1937) 226–240.

[71] I.S. Edelmann, J. Liebmann, Anatomy of body water and electrolytes, Am. J. Med. 27 (1959) 256–277.

[72] H.M. Jones, K. Mayawala, P. Poulin, Dose selection based on physiologically based pharmacokinetic (PBPK) approaches, AAPS. J. 15 (2013) 377-87.

[73] J.S. Barrett, O. Della Casa Alberighi, B. Läer S, Meibohm, Physiologically based pharmacokinetic (PBPK) modeling in children, Clin. Pharmacol. Ther. 92 (2012) 40-9.

[74] G. Lu, K. Abduljalil, M. Jamei, T.N. Johnson, H. Soltani, A. Rostami-Hodjegan, Physiologically-based pharmacokinetic (PBPK) models for assessing the kinetics of xenobiotics during pregnancy: achievements and shortcomings, Curr. Drug. Metab. 13 (2012) 695-720.

[75] C.M. Thompson, D.O. Johns, B. Sonawane, H.A. Barton, D. Hattis, R. Tardif, K. Krishnan, Database for physiologically based pharmacokinetic (PBPK) modeling: physiological data for healthy and health-impaired elderly, J. Toxicol. Environ. Health. B. Crit. Rev. 12 (2009) 1-24.

[76] M. Chenel, F. Bouzom, F. Cazade, K. Ogungbenro, L. Aarons, F. Mentré, Drug-drug interaction predictions with PBPK models and optimal multiresponse sampling time designs: application to midazolam and a phase I compound. Part 2: clinical trial results, J. Pharmacokinet. Pharmacodyn. 35 (2008) 661-81.

[77] J.C. Lipscomb, S. Haddad, T. Poet, K. Krishnan, Physiologically-based pharmacokinetic (PBPK) models in toxicity testing and risk assessment, Adv. Exp. Med. Biol. 745 (2012) 76-95.

[78] P. Ruiz, M. Ray, J. Fisher, M. Mumtaz, Development of a human Physiologically Based Pharmacokinetic (PBPK) Toolkit for environmental pollutants, Int. J. Mol. Sci. 12 (2011) 7469-80.

[79] J.B. Knaak, C.C. Dary, F. Power, C.B. Thompson, J.N. Blancato, Physicochemical and biological data for the development of predictive organophosphorus pesticide QSARs and PBPK/PD models for human risk assessment, Crit. Rev. Toxicol. 34 (2004) 143-207.

[80] Haagard, H. W. The absorption, distribution and elimination of ethyl ether, J. Biol. Chem. 59(1924):753-770.

[81] I. Nestorov, Whole body pharmacokinetic models, Clin. Pharmacokinet. 42(2003):883-908.

[82] W. Schmitt, S. Willmann, Physiology-based pharmacokinetic modeling: ready

to be used, Drug. Discov. Today. Technol. 2 (2005):125-132.

[83] L. Liu, K. S. Pang, An integrated approach to model hepatic drug clearance, Eur. J. Pharm. Sci. 29(2006):215-230.

[84] P. Zhao, L. Zhang, J.A. Grillo, Q. Liu, J.M. Bullock, Y.J. Moon, P. Song, S.S. Brar, R. Madabushi, T.C. Wu, B.P. Booth, N.A. Rahman, K.S. Reynolds, E. Gil Berglund, L.J. Lesko, S.M. Huang, Applications of physiologically based pharmacokinetic (PBPK) modeling and simulation during regulatory review, Clin. Pharmacol. Ther. 89 (2011):259-67.

[85] J. H. Lin, Y. Sugiyama, In vitro and in vivo evaluation of the tissue-to-blood partition coefficient for physiological pharmacokinetic models, J. Pharmacokinet. Biopharm. 10 (1982):637-647.

[86] Y. Naritomi, S. Terashita, Prediction of human hepatic clearance from in vivo animal experiments and in vitro metabolic studies with liver microsomes from animals and humans, Drug. Metab. Dispos. 29 (2001):1316-24.

[87] M.O. Fouch´ecourt, M. B´eliveau, K. Krishnan, Quantitative structure-pharmacokinetic relationship modelling, Sci. Total. Environ. 274 (2001):125-135.

[88] H. Tang, M. Mayersohn, A novel model for prediction of human drug clearance by allometric scaling, Drug. Metab. Dispos. 33 (2005):1297 – 1303.

[89] L.R. Williams, R.W. Leggett, Reference values for resting blood flow to organs of man, Clin. Phys. Physiol. Meas. 10 (1989):187-217.

[90] R. Price, R. Conolly, Modeling interindividual variation in physiological factors used in PBPK models of humans, Crit. Rev. Toxicol. 33 (2003):469-503.

[91] F.F. Farris, R.L. Dedrick, F.G. King, Cisplatin pharmacokinetics: applications of a physiological model, Toxicol Lett. 43 (1988):117-37.

BIOGRAPHICAL SKETCH

Di Bei was born in November 1984, in Chengdu, China. She earned her bachelor's degree in pharmacy in Sichuan University in 2007. She further accomplished the master's degree in pharmaceutical sciences in 2009 from University of Missouri-Kansas City with the thesis on cubosomes. Before she joined PhD program in University of Florida, she acquired the Statistical Minor in Data Analysis. She accomplished her PhD study from Dr. Derendorf's lab and received her Doctor of Philosophy degree in pharmaceutical sciences in December 2015.